

Referee #3:

**General comments:** Previous works have also fitted the CTI products to functions that represent a grid cell CTI value, such as in Kleinen et al., 2012 and Ringeval et al., 2012. Although this approach sounds reasonable, I am not convinced that by providing the inundated fraction in the grid cell the computational cost is considerably reduced. This might be true for some models but not in all cases and not in all resolutions. Furthermore, if this is true, an extra preprocessing of after the CTI grid cell fitting to obtain the inundated fraction implies an extra step beforehand that certainly adds more errors in the model input. The authors give a step towards this by reducing the uncertainties in the calculation of the maximum soil saturated fraction obtained from the CDFs, by introducing a parameterization to calibrate the maximum wetland fraction ( $F_{\max}^{\text{wet}}$ ) with “original” values ( $F_{\max}$ ) obtained from the CDF when the mean CTI is zero.

An interesting contribution from this manuscript is the comparison of the three DEM's (HYDRO1k, GMTED and HydroSHEDS) for wetland simulation in DGVMs, and arise the need of hydrological corrections before its use.

My major concern regarding this manuscript is that I find it still too descriptive for the model setup and I believe is still out of the scope of Biogeosciences. Despite the authors made an effort by adding few sentences regarding the analysis of modeled methane fluxes to test the wetland representation from the model, the authors rarely refer to the CH<sub>4</sub> fluxes application throughout the manuscript. The focus of the manuscript is still to simply compare the three DEM products in their model setup and improve the  $F_{\max}$  parameter in TOPMODEL, but they do not make any strong reference to the evaluation of methane fluxes or discuss further other papers that make this analysis. A clear example of this, are in the specific aims of the manuscript listed at the end of section 1, which are only focused on model improvement based on the analysis of using three different DEM's. Also in Discussion and Conclusions there is nothing regarding methane emissions. Therefore, I still find difficult to agree that this manuscript should be published in Biogeosciences in the current state, and I believe is still suitable for GMD.

Despite this, I made some comments that the authors may find useful to improve the current version of the manuscript. Some of the statements made by the authors are ambiguous and it needs several language corrections, this makes it sometimes hard to understand what the authors really mean. The wording is particularly hard to follow in the Discussions sections, although I make some specific comments, I suggest that the authors revise carefully their sentences and re-arrange the wording for a clearer reading.

Still if there error are corrected, and comments here included answered, I encourage the authors to make more emphasis in the CH<sub>4</sub> fluxes, e.g. include a specific aim in section 1 and discuss further other works that had published CH<sub>4</sub> fluxes using similar approaches (e.g. Kleinen et al., 2012). Also compare to more representative studies for the regions of interest with other methodologies (see my comments below for this). Therefore, I cannot support at this point the publication of this manuscript in its current form in Biogeosciences.

In terms of potential errors that might be introduced during preprocessing of TOPMODEL parameters as reviewer mentioned, we would like to clarify that there is no additional errors introduced in the processes, this is because the discrete cumulative distribution function (CDF) was used to derive original  $F_{\max}$  instead of using fitted CDF curve. For computational efficiency, we admitted that our approach might not be applicable at all resolutions (especially for researches at fine resolutions), but for applications at coarse resolutions in Earth System Models, it is an essential step to save computational time since there are  $\sim 10^4$  pixels (if use DEM at 500 m resolution) within  $0.5^\circ$  grid cell and the discrete cumulative distribution of all the sub-grids need to be calculated at each time step.

For the analysis of methane fluxes, we strengthened the discussions regarding the sensitivity of  $\text{CH}_4$  emissions to TOPMODEL parameterizations by comparing global and regional estimates of  $\text{CH}_4$  emission among model experiments. In evaluation part section 4.1, the importance of  $F_{\max}$  calibration in  $\text{CH}_4$  estimation was justified, and then a new Table 5 was added to summarize the differences. The new statements are listed below:

Page 17, Line 702:

*In addition, TOPMODEL parameterizations have considerable influence on simulated  $\text{CH}_4$  fluxes that the uncertainty of mean annual  $\text{CH}_4$  emissions from topography inputs is estimated to be  $29.0 \text{ Tg yr}^{-1}$  (Table 5). All of the model estimates generally fall within the range of inversion estimates. The differences of  $\text{CH}_4$  emissions among the model experiments is related to simulated magnitude of wetland extents because the fraction of  $\text{CH}_4$  emissions from tropics ( $\sim 63\%$ ) and Extratropics ( $\sim 27\%$ ) keep constant due to same parameters  $r_{\text{C:CH}_4}$  and  $f_{\text{ecosys}}$ . The importance of hydrological correction is highlighted by results based on GMTED, suggesting that applying topography map without hydro-correction may potentially underestimate  $\text{CH}_4$  fluxes due to lower hydrological connectivity that dampen generating of inundation. In addition, fine-scale topography data like HydroSHEDS show higher  $\text{CH}_4$  fluxes than HYDRO1k, suggesting its influence on capturing small wetlands/inundated areas that may be ignored by coarse-resolution products.*

Table 5. List of global and regional wetland CH<sub>4</sub> estimates from our model experiments (see Table 2) over the period 1980-2000. All units are Tg CH<sub>4</sub> yr<sup>-1</sup>±1σ, where standard deviation represents the interannual variation in the model estimates. Note that estimates from some reference studies are not for the same period.

Estimates	Global	Regions			Hotspot			
		Tropics (20N-30S)	Temperate (20-45N, 30S-50S)	Northern (>45N)	Central Amazon <sup>b</sup>	WSL	Hudson Bay	Alaska
SHEDS_BASIN	171.9	109.3±2.3	26.4±1.0	36.1±1.8	10.9±0.3	5.4±0.9	6.5±0.5	1.7±0.3
SHEDS_GRID	193.0	123.7±2.2	31.4±1.0	38.7±1.9	11.4±0.3	5.5±0.9	7.1±0.6	1.5±0.3
GMTED_BASIN	130.1	85.5±2.3	19.0±0.9	26.3±1.4	9.5±0.4	4.5±0.9	4.4±0.6	1.6±0.3
GMTED_GRID	117.2	76.7±2.3	16.4±0.9	24.2±1.4	9.2±0.4	4.1±0.9	4.2±0.6	1.4±0.3
HYDRO1K_BASIN	148.3	96.4±2.3	21.5±0.9	30.3±1.6	10.4±0.3	4.4±0.9	5.8±0.6	1.7±0.3
HYDRO1K_GRID	128.8	85.0±2.3	17.8±0.9	26.0±1.4	10.0±0.4	3.9±0.9	4.8±0.6	1.5±0.3
Melton et al. (2013) <sup>a</sup>	190±39						5.4±3.2	
Zhu et al. (2015)	209-245			38.1-55.4				
Chen et al. (2015)				35			3.11±0.45	
Zhu et al. (2014)				34-58			3.1±0.5	
Ringeval et al. (2012)	193.8	102	51	40.8				
Glagolev et al. (2011)						3.91±1.3		
Melack et al. (2004)					9.1			
Zhuang et al. (2004)				57.3				
Chang et al. (2014)								2.1±0.5
Bloom et al. (2012)		111.1						
Bousquet et al. (2011)	151±10	91±11						
Bloom et al. (2010)	165±50	91±28					4.9±1.4	

<sup>a</sup> WETCHIMP estimates for 1993-2004

<sup>b</sup> Central Amazon (54-72°W,0-8°S)

In the new version of the manuscript, we've clarified some points in Discussions. Please see below responses.

### Major comments:

- The full name of an acronym should be always stated when is first mentioned in the paper. I could not find the full name of LPJ-wsl or LPJ-DGVM, please write it in full either in the Abstract or in the Introduction when is first mentioned (P17957, L23?). There are also other acronyms that should be written its name in full, please check this throughout the manuscript.

### Revised

- L14 – In the sentence: "... which has been proven to at least partly cause biases due to limited spatial resolution...", I don't think 1km is a limited spatial resolution for such datasets, please elaborate here what the authors really mean with these sentence.

L26 – mention some examples of physical processes the authors refer to in this line (e.g.)

The sentence has been changed to read:

Page 3, Line 120:

*Among all parameters in TOPMODEL, the Compound Topographic Index (CTI) is of critical importance for determining inundated areas in terrain-related hydrological applications (Ward and Robinson, 2000; Wilson and Gallant, 2000). It measures the relative propensity for soils to become saturated (Beven and Cloke, 2012) and consequently it drives the accuracy of wetland area scaled to the larger grid cell (Ducharne, 2009; Mulligan and Wainwright, 2013). Although the importance of CTI has been highlighted, only few studies have so far evaluated the effect of CTI on modelling the spatial and temporal patterns of global wetland dynamics. This is due to a limited availability of global CTI products. During the last decade, the first CTI product at 1km resolution from HYDRO1k global dataset released by U.S. Geological Survey (USGS) in 2000 has become the most commonly applied global dataset for large-scale applications (Kleinen et al., 2012; Lei et al., 2014; Ringeval et al., 2012; Wania et al., 2013). However, HYDRO1k has been proven to potentially overestimate inundation extent due to the quality of the underlying digital elevation model (DEM) (Grabs et al., 2009; Lin et al., 2010; Lin et al., 2013; Sørensen and Seibert, 2007;). With recent development of DEMs (Danielson and Gesch, 2011; Lehner et al., 2008), there is a requirement to investigate uncertainties caused by CTI parameter.*

L26 we add: (e.g. snow aging effect on thermal properties)

P17967-L26; P17968, L1-2. Although the correlation between the model simulated frozen-days and the in Fig. 3 agrees well, the authors speculate that the low correlation in East Siberia could be due to the nature of the data, while in the satellite observations it is included the ice condition in the vegetation canopy, snow layer and frozen water in the upper soil layer, in the model it is only considered the frozen state of the top soil, but if this is true, why in the

southern regions of Siberia the correlation seems to agree better? I would expect that this behavior remain at least in most part of northern latitudes.

Thanks for pointing out this issue. The low correlation in some arctic regions was due to the insulation of soil temperature. This is because in our model, frozen day is calculated in condition that unfreezing water fraction is close to zero in all of the upper soil layers. When there is a large amount of snow above surface, the timing of soil temperature to reach frozen status will be delayed due to extreme high snow depth in those regions.

The sentence has been revised as:

Page 11. Line 437:

*The lower correlation in East Siberia probably originates from two issues: high snow depth in LPJ-wsl that insulates soil temperature and consequent delay of soil temperature to reach complete freezing; and the relatively large uncertainty of FT-ESDR derived soil frozen status in those regions (Kim et al., 2012).*

- It is misleading the explanation of  $F_{\max}$  and  $F_{\max}^{\text{wet}}$ . To what I understood from the manuscript,  $F_{\max}$  is taken for the satellite observations and used to calibrate  $F_{\max}^{\text{wet}}$  which is then used to obtain the wetland area fraction  $F_{\text{wet}}$ . However, the authors repeat in the manuscript that what they propose is a “calibration of  $F_{\max}$ ”, shouldn’t be  $F_{\max}^{\text{wet}}$ ? Please correct me if I am wrong or otherwise, be more explicit and careful in the description of the method and correct where necessary in the manuscript.

To avoid misunderstanding and for consistence with other studies, the  $F_{\max}^{\text{wet}}$  has been replaced with  $F_{\max}$  to make it clear.

- The newly available DEM product from the Centre for Ecology and Hydrology (an improvement from HYDRO1k from 30” res to 15” res) <https://data.gov.uk/dataset/high-resolution-global-topographic-index-values1>, should be at least mentioned and discuss how this new product can improve the representation of wetlands at global scale and how this can be combined with the  $F_{\max}$  (or  $F_{\max}^{\text{wet}}$ ?) calibration proposed in this manuscript.

Sorry we didn’t find the DEM dataset from the website you provided. If the new topographic index product based on HydroSHEDS DEM is what you mean, we added sentence to describe this dataset. We didn’t use this new dataset because we need to keep all the topographic maps generated from the three DEMs in our model experiments following the same algorithm to make it comparable. Below is the description:

Page 8 Line 334:

*To avoid mismatch of CTI value inherent in computing CTI with different CTI algorithms, we generated a global CTI map based on the three DEM products, instead of relying on existing CTI products (e.g. HYDRO1k CTI, HydroSHEDS CTI product from Centre for Ecology and Hydrology (Marthews et al., 2015)).*

**Specific comments:**

P17954,

L2 – spatio-temporal

L16 – Define here what DEM stands for

Revised

P17957,

L10 – Add citation year for Ward and Robinson (2000)

L12 – is really 1 km limited?

L26 – e.g. physical processes

Revised

P17958,

L16-17 – remove parenthesis in Hodson et al., 2011 AND Wania et al., 2013

L17 – “and is a function of two scaling ...”

L17 – the authors does not define  $f_{\text{ecosys}}$  and  $r_{\text{CH}_4:\text{C}}$  in the text, nor say how they are obtained

L24 – delete “contributed as”

Revised

P17959,

L18 – move parentheses before “Cosby” to before “1984” (Cosby et al., (1984))

Revised

P17960,

L20 – add in parenthesis after the name the acronym CTI

Revised

P17961,

L14 – delete “furthermore”

L18 – to my understanding a gamma function can be also exponential, and this in the end is a similar treatment than the gamma function, thus not reducing the computational cost.

Revised

P19762,

L3 – “... topographic information generated by fitting the ...”

L4 – add a comma after CTI

L4 – here the authors should be more specific on “observed maximum wetland fraction” starting that this information was obtained

L15 – write the meaning here of SWAMPS-GLWD

Revised

P17963,

L4 – write the meaning of HWSD

L4 – reference for the HWSD soil texture database?

L8 – replace “more” by “mainly”

L10 – latitudes

L19 – write the spatial resolution of the DEMs after they are mentioned in the following lines

Revised

P17964,

L14-20 – Here it is a misleading whether the authors generated ONE single CTI maps based on the three DEM products or if there were THREE CTI maps been one per DEM product. This becomes confusing along the manuscript, particularly arriving at Figure 7. See my comment below for it.

L20-25 – Here it is not really clear in the paragraph if GMTED was also used to generate the global CTI map despite was not hydrologically corrected as the other two DEM products? What do the authors mean with “retaining GMTED DEM without hydrologically correction”?

L25 – change “hydrologically” by “hydrological”

We made some revision to make it clear. We generated three CTI map based on three DEM products with same algorithm. Here below is revision:

Page 8 Line 334:

*To avoid mismatch of CTI value inherent in computing CTI with different CTI algorithms, we generated three global CTI maps based on the three DEM products, instead of relying on existing CTI products (e.g. HYDRO1k CTI, HydroSHEDS CTI product from Centre for Ecology and Hydrology (Marthews et al., 2015)). Since studies show that multiple flow direction algorithms for calculating CTI give better accuracy compared with single-flow algorithms in flat areas (Kopecký and Čížková, 2010; Pan et al., 2004), thus we selected an algorithm from R library ‘topmodel’ (Buytaert, 2011), which applies the multiple flow routing algorithm of Quinn et al. (1995) to calculate the global CTI maps. The DEMs from HYDRO1k and HydroSHEDS had been previously processed for hydrological-correction, meaning that the DEMs were processed to remove elevation depressions that would cause local hydrologic ‘sinks’. To include a comparison of (hydrologically) corrected and uncorrected DEMs in our analyses as some studies have been done previously (Stocker et al., 2014), the GMTED DEM was applied without hydrological correction.*

P17965,

L4 – “generating a global catchment map”

L9 – “The description of the DEM products used in this study are summarized in Table 2”

L13 – here the word spin up is separated, while in L18 is a single one (spinup), the correct should be separated

Revised

P17966,

L27 – Poulter et al., 2015

Revised

P17967,

L24 – “in those regions”

Revised

P17969,

L4 – correct here and throughout the manuscript that CH<sub>4</sub> is with subscript (i.e. CH<sub>4</sub>)

L5-10 –As stated in the caption of Figure 6, the authors should mention here the DEM product used is Hydro-SHDES for TOPMODEL. However, this is confusing since earlier in the manuscript the authors mention that they generate a mean CTI map of the three DEM products to actually “calibrate” TOPMODEL, so why here it is only comparing Hydro-SHEDS?

L5-10 – I would try to avoid using the expression “calibrated TOPMODEL” and “non-calibrated TOPMODEL” for the correction on the maximum fraction of wetland extent. This is what it was actually corrected ( $F_{max}$ ) but TOPMODEL itself not only provides the maximum fraction.

L14-19 – I am not convinced with the comparison of results from the West Siberian Lowland to the CARVE observations in Alaska. Although both are boreal wetland regions, there are published works that match better the region of interest in question. I would rather use for example previous observations at least in the Siberian region with other techniques like Eddy covariance like the works of Parmentier et al., 2011 (J. of Geophys. Res.) or Wille et al., 2008 (Global Change Biology).

L22-25 – Figure 7 is really well explained here nor in the Figure caption. What do the authors mean with the prefix BASIN and GRID? This part needs more detailed information in the simulations description before it is presented in the results. If they are the aggregation schemes they briefly mention in the introduction, then the authors need to refer to them by their name there. Furthermore, the authors mention “both datasets” but they should be specific to what they mean (e.g. the results from the simulations with BASIN and GRID aggregation schemes?). I honestly, don't see much the sense of this figure plus it is hard from it to visually look at the “uncertainties” of the parameterization.

L27 – replace “differing” by “different”

We agree that evaluating our CH<sub>4</sub> fluxes with independent estimates from flux tower measurement or airborne campaigns is important but we found it is

difficult to directly apply Eddy Covariance results in evaluations as there is scale mismatch between model estimates at 0.5 degree resolution and flux tower results at  $\sim 1\text{-}10\text{ km}^2$ . Upscaling point measurements might introduce large uncertainties due to the influence of spatial heterogeneity. The measurements conducted over broad areas such as aircraft can span similar temporal and spatial scale as our model results and is independent.

W revised a few sentences in this paragraph to make it clear:

Page 12. Line 479:

*To evaluate the effect of  $F_{\max}$  calibration on  $\text{CH}_4$  emission estimates, two estimates of  $\text{CH}_4$  (with and w/o calibration) over the WSL regions were compared with observation-based estimate from Glagolev et al. (2011) (Figure 6). The 3-year mean annual total emission from original version is  $6.29 \pm 0.51\text{ Tg CH}_4\text{ yr}^{-1}$ , falling into the upper part of range from land surface models and inversions (Bohn et al., 2015), whereas the calibrated version is close to the estimate of Glagolev et al. (2011) ( $3.91 \pm 1.29\text{ Tg CH}_4\text{ yr}^{-1}$ ) with  $4.6 \pm 0.45\text{ Tg CH}_4\text{ yr}^{-1}$ . In addition, the spatial pattern of  $\text{CH}_4$  emission with  $F_{\max}$  calibration shows better agreement with observation than non-calibration one with relatively larger emissions in Taiga forests and central region ( $55\text{-}65^\circ\text{N}$ ,  $65\text{-}85^\circ\text{E}$ ). We also compared our estimates with recent airborne campaign observations for Alaska during 2012 growing seasons. Estimates with  $F_{\max}$  calibration also falls well into the range of recent estimate ( $2.1 \pm 0.5\text{ Tg CH}_4\text{ yr}^{-1}$ ) for Alaska based on airborne observations (Chang et al., 2014) with a total of  $1.7\text{ Tg CH}_4\text{ yr}^{-1}$  during 2012 growing season ( $3.1\text{ Tg CH}_4\text{ yr}^{-1}$  from non-calibrated estimate), indicating necessity of  $F_{\max}$  calibration to accurately capture annual  $\text{CH}_4$  emission and spatial variability for boreal wetlands.*

L22-25: We added descriptions in caption of Figure 7 and rearranged Section 3.1 and 3.2 to make the description easier to follow:

Page 9 Line 364:

*One of key assumptions in TOPMODEL is that the water table is recharged at a spatially uniform and steady rate with respect to the flow response timescale of the catchment (Stieglitz et al., 1997). Given the fact that we consider the water to be stagnant within each grid, the mean CTI parameter was estimated with two alternative schemes: (1) a regular 'grid-based' or gridded approach, i.e., the subgrid CTI values were averaged per  $0.5^\circ$  grids, and (2) an irregular 'basin-based' approach, where mean CTI were calculated over the entire catchment area in which the respective pixel is located. For generating a global catchment map at  $0.5^\circ$  resolution, we applied a majority algorithm in the case of multi-catchments in a grid with consideration of avoiding isolated pixels for specific river basin. There are two catchment area products applied in this study, HYDRO1k (2013) and HydroSHEDS. Similarly, the parameter  $C_s$  was generated using nonlinear least squares estimates from both of these two different CTI calculation strategies. Two sets of model experiments were carried out to compare the wetland dynamics under basin and grid-based TOPMODEL parameterizations respectively (Table 2).*

P17970,

L5 – replace “sensitivity” by “sensible”

L10-12 – I thought GMTED was not hydrologically corrected?

L11 – Add the degrees symbol to 60N

L16-17 – replace “estimation” by “estimates”

L18 – replace “paddy” by “paddies”

L21 – replace “digitalized” by “digitized”

L22 – move the word “directly” after “... when comparing ...” at the end of line 20

L25 – I guess it should say “... due to permanent wetlands that are hard to detect by GIEMS.”

L27 – please elaborate here more about the satellite inundation datasets, what the authors really mean with “non-specific measurement of inundation”?

L28 – This paragraph is also misleading, do the authors meant to say that the definition of wetland in this work is in agreement to the definition used by the National Wetlands Working Group? Please also reference this in the reference section as: National Wetland Working Group, 1988. Wetlands of Canada, Ecological Land Classification Series, No., 24. Canada Committee on Ecological Land Classification. Sustainable Development Branch, Environment Canada and Polyscience Publications Inc. Montreal, Quebec, Canada.

We changed the sentence as below:

Page 13, Line 515: *Note that GMTED is derived from the same DEM product SRTM as HydroSHEDS but without hydro-correction, indicating the importance of hydro-correction in simulating spatial patterns of wetlands.*

Page 13, Line 532: *Remotely sensed inundation datasets emphasizes on open water while wetland area in our study is specifically defined from inventories following the National Wetlands Working Group (1988) classification that include peatlands, mineral wetlands, and seasonally inundated shallow waters.*

L28: We also add reference in reference section.

P17971,

L7 – SON is not a season but the acronym of a list of months that accumulated corresponds to a season (autumn), please rephrase correctly (replace the word seasons by months).

L9 – what do the authors mean here with “masked estimates”? ambiguous

L10 – pluralize latitude

L11 –an area cannot be higher, only larger

L12 – rephrase, seasons are not unfrozen, you can instead say “... from longer periods of unfrozen and relatively water saturated soil in the model data”

L16 – replace “seasons” by “months” (or “SON seasons” by “autumn”)

L22 replace “underestimated” by “underestimates”

L24 – replace “estimates” by “data sets”

L24 – replace “base” by “based”

Revised

P17972,

L4 – here the authors refer to the “grid” experiments as “tile-based”, please keep consistency with your nomenclature here and throughout the manuscript

L10 – “the” Pearson’s correlation coefficient

L13 – Define what is a “Transcom region”?, it was only mentioned before in the figure caption of Fig. 2 and also in caption of Fig. 8

L17-18 – This sentence is a confirmation of previous works, like Kleinen et al., 2012. Taking this into account I would rather make more emphasis throughout

the manuscript that the aim of the correction in the maximum wetland extent is to actually improve the representation of wetlands by the models using TOPMODEL at a regional scale. This has to be highlighted even in the abstract section.

Revised

Thanks for your comments. We've added sentences in abstract to highlight it as below:

Page 1 Line 38: *This study demonstrates the feasibility of TOPMODEL to capture spatial heterogeneity of inundation at large scale and highlights the significance of correcting maximum wetland extent to improve modeling of interannual variations in wetland areas.*

P17973

L7-8 – wording of sentence a bit strange, I suggest: “... TOPMODEL with calibrated parameters as described in this study, allows the dynamical simulation of wetlands, in particular their geographic location and extent.”

L9-13 – this sentence is particularly hard to follow, please re-arrange the wording to make it clearer

L21 – strange wording, do the authors mean: “... in absolute values, which is necessary for global wetland modeling.”? I would modify this sentence since it is confusing in the way it is written now.

L23 – change to: “...because the physical processes are described in a robust way”

L25 – “allows the retrieval of the maximum water saturated fraction ( $F_{max}$ ) of a model grid cell, which is defined by ...”

This paragraph was changed to:

Page 15 Line 604:

*The coupling between LPJ-wsl and TOPMODEL with calibrated parameters as described in this study, improves the dynamical simulation of wetlands, in particular their geographic location and extent. This is based on the recent discussions of the suitability of TOPMODEL applications to simulate wetland variations at large spatial scale (Ringeval et al., 2012), and intercomparisons of the wetland-area-driven model bias in CH<sub>4</sub> emission at regional scale (Bohn et al., 2015a). The large discrepancies of wetland area among LSMs so far have shown extensive disagreement with inventories and remotely sensed inundation datasets (Melton et al., 2013), which is partly due to large varieties of schemes used for representing hydrological processes, or due to the parameterizations for simulating inundations. Our results suggest that benchmarking  $F_{max}$  is necessary for global wetland modelling.*

P17974,

L2 – Replace “This” by “The”

L14 – pluralize “application”

L15 – pluralize “parameterization”

L16 – “fine scale”

L16 – “which complicates the comparison to inventories”

L17-22 – the wording of this paragraph is wrong, and hard to follow, please correct it.

Revised paragraph is below:

Page 16, Line 641:

*Integration of satellite-based and inventory-based observations to calibrate  $F_{max}$  is highlighted in this study. Combining SWAMPS and GLWD led to simulated wetland area consistent with detailed regional distribution (Poulter et al., in preparation). Our estimation of global wetland potential/maximum is  $\sim 10.3$  Mkm<sup>2</sup>, and in agreement with the deduction (10.4 Mkm<sup>2</sup>) from recent estimates at finer resolution for total open water ( $\sim 17.3$  Mkm<sup>2</sup>) (Fluet-Chouinard et al., 2015), lakes ( $\sim 5$  Mkm<sup>2</sup>) (Verpoorter et al., 2014), and rice paddies (1.9 Mkm<sup>2</sup>) (Leff et al., 2004). The calibration of  $F_{max}$  maintains capability of simulating the wetland dynamics on decade-to-century long time scales. As shown in Figure 9, the wetland potential for permafrost and arid/semi-arid regions is high. Even in tropical regions, there is  $\sim 20$ -30% of potential areas can be inundated.*

P17975,

L14 – “... size and location that make hard to reconcile a single definition for wetlands”

L15 – pluralize “parameterization”

L19 – pluralize “area”

L25 – elaborate in “limitation therein”

L18 – and complete paragraph should be moved to the introduction since this is a better start for the background knowledge and motivation of this study. This paragraph will certainly improve the flow of the method if it is moved forward in the manuscript.

L26 – move “during the last decade” to the beginning of the sentence

We moved the paragraph to Introduction and revised Introduction section to improve the flow. Here below is revised part of Introduction:

Page 3, Line 117:

*While prognostic wetland dynamics schemes are promising to resolve these observational issues, the configuration parameters for TOPMODEL are a potential source of uncertainty in estimating wetland dynamics (Marthews et al., 2015). Among all parameters in TOPMODEL, the Compound Topographic Index (CTI) is of critical importance for determining inundated areas in terrain-related hydrological applications (Ward and Robinson, 2000; Wilson and Gallant, 2000). It measures the relative propensity for soils to become saturated (Beven and Cloke, 2012) and consequently it drives the accuracy of wetland area scaled to the larger grid cell (Ducharne, 2009; Mulligan and Wainwright, 2013). Although the importance of CTI has been highlighted, only few studies have so far evaluated the effect of CTI on modelling the spatial and temporal patterns of global wetland*

*dynamics. This is due to a limited availability of global CTI products. During the last decade, the first CTI product at 1km resolution from HYDRO1k global dataset released by U.S. Geological Survey (USGS) in 2000 has become the most commonly applied global dataset for large-scale applications (Kleinen et al., 2012; Lei et al., 2014; Ringeval et al., 2012; Wania et al., 2013). However, HYDRO1k has been proven to potentially overestimate inundation extent due to the quality of the underlying digital elevation model (DEM) (Grabs et al., 2009; Lin et al., 2010; Lin et al., 2013; Sørensen and Seibert, 2007;). With recent development of DEMs (Danielson and Gesch, 2011; Lehner et al., 2008), there is a requirement to investigate uncertainties caused by CTI parameters.*

P17976,

L2 – “from regional to global scales”

L2 – The reference Lin et al., must be separated as: Lin et al., 2010; Lin et al., 2013; the first one corresponds to Kairong Lin and the second to a different author (Shengpan Lin)

L6 – “benefit”

L7 – “creating a more realistic representation ...”

L9 – “This is supporting the ideas of ...”

L16 – “closed depressions”

L24 – “As a result”

Revised

P17977,

L23 – “describe”

L25 – “need”

Revised

P17978,

L27-28 – “Remotely sensed global inundation is prone to underestimate small wetland areas, ...”

Revised

P17979,

L3 – “This raises the need for benchmark dataset useful to generate accurate products with lower uncertainties”

L14 – “and captured well the spatio-temporal ...”

Revised

References

P17980,L24 – Update the reference by Bohn et al., 2015a (not in discussion anymore)

Missing reference USGS, 2000 (cited in P17964, L5-6)

## Revised

### Figures

Besides specific comments on figures' captions mentioned before, here are some more comments.

Figure 1 – replace the symbol lambda with the horizontal line on top by lambda with subscript m as in the text. Also in the label of the x-axis lambda should have the subscript l corresponding to the local CTI value. Change this also in the legend of the figure

Figure 2 – the figure caption must be considerably improved, by making reference to the panels and their meaning, also by editing the text (italics, subscripts, etc.)

Figure 4 – add year “Tanocai2009” in both title of subplot and caption

Figure 5 – include in the caption the area of study (e.g. Amazon River Basin or Lowland Amazon Basin)

Figure 6 – Change the units of CH<sub>4</sub> emissions with the area unit before the time unit (e.g. g CH<sub>4</sub> m<sup>-2</sup> yr<sup>-1</sup>)

Figure 8 – replace “variation” by “variability”

## Revised

Caption of Figure 2 was changed to:

*Figure 2. TOPMODEL parameter maps in model experiments. Mean CTI (a, b) and C<sub>s</sub> (c, d) aggregated by river basin (denoted as “By Basin”) and by grid cell (denoted as “By Tile”) schemes from HydroSHEDS were listed. F<sub>max</sub> (e) for calibration was generated using SWAMPS-GLWD and GLWD. Map of regions (f) was used to partition globe into boreal, temperate, tropical biomes (Gurney et al. 2003).*

Part of updated references:

### References:

Bloom, A. A., Palmer, P. I., Fraser, A., and Reay, D. S.: Seasonal variability of tropical wetland CH<sub>4</sub> emissions: the role of the methanogen-available carbon pool, *Biogeosciences*, 9, 2821-2830, 2012.

Bloom, A. A., Palmer, P. I., Fraser, A., Reay, D. S., and Frankenberg, C.: Large-Scale Controls of Methanogenesis Inferred from Methane and Gravity Spaceborne Data, *Science*, 327, 322-325, 2010.

Bohn, T. J., Melton, J. R., Ito, A., Kleinen, T., Spahni, R., Stocker, B. D., Zhang, B., Zhu, X., Schroeder, R., Glagolev, M. V., Maksyutov, S., Brovkin, V., Chen, G., Denisov, S. N., Eliseev, A. V., Gallego-Sala, A., McDonald, K. C., Rawlins, M. A., Riley, W. J., Subin, Z. M., Tian, H., Zhuang, Q., and Kaplan, J. O.: WETCHIMP-WSL: intercomparison of wetland methane emissions models over West Siberia, *Biogeosciences*, 12, 3321-3349, 2015.

Bousquet, P., Ringeval, B., Pison, I., Dlugokencky, E. J., Brunke, E. G., Carouge, C., Chevallier, F., Fortems-Cheiney, A., Frankenberg, C., Hauglustaine, D. A.,

Krummel, P. B., Langenfelds, R. L., Ramonet, M., Schmidt, M., Steele, L. P., Szopa, S., Yver, C., Viovy, N., and Ciais, P.: Source attribution of the changes in atmospheric methane for 2006–2008, *Atmos. Chem. Phys.*, 11, 3689-3700, 2011. Buytaert, W.: <http://cran.r-project.org/web/packages/topmodel/index.html>, last access: (February 2015) 2015.

Chang, R. Y.-W., Miller, C. E., Dinardo, S. J., Karion, A., Sweeney, C., Daube, B. C., Henderson, J. M., Mountain, M. E., Eluszkiewicz, J., Miller, J. B., Bruhwiler, L. M. P., and Wofsy, S. C.: Methane emissions from Alaska in 2012 from CARVE airborne observations, *Proceedings of the National Academy of Sciences*, doi: 10.1073/pnas.1412953111, 2014. 2014.

Chen, X., Bohn, T. J., and Lettenmaier, D. P.: Model estimates of climate controls on pan-Arctic wetland methane emissions, *Biogeosciences*, 12, 6259-6277, 2015.

Glagolev, M., Kleptsova, I., Filippov, I., Maksyutov, S., and Machida, T.: Regional methane emission from West Siberia mire landscapes, *Environmental Research Letters*, 6, 045214, 2011.

Glagolev, M., Kleptsova, I., Filippov, I., Maksyutov, S., and Machida, T.: Regional methane emission from West Siberia mire landscapes, *Environmental Research Letters*, 6, 045214, 2011.

Harris, I., Jones, P. D., Osborn, T. J., and Lister, D. H.: Updated high-resolution grids of monthly climatic observations – the CRU TS3.10 Dataset, *International Journal of Climatology*, 34, 623-642, 2014.

Kopecký, M. and Čížková, Š.: Using topographic wetness index in vegetation ecology: does the algorithm matter?, *Applied Vegetation Science*, 13, 450-459, 2010.

Marthews, T. R., Dadson, S. J., Lehner, B., Abele, S., and Gedney, N.: High-resolution global topographic index values for use in large-scale hydrological modelling, *Hydrol. Earth Syst. Sci.*, 19, 91-104, 2015.

Melack, J. M., Hess, L. L., Gastil, M., Forsberg, B. R., Hamilton, S. K., Lima, I. B. T., and Novo, E. M. L. M.: Regionalization of methane emissions in the Amazon Basin with microwave remote sensing, *Global Change Biology*, 10, 530-544, 2004.

Pan, F., Peters-Lidard, C. D., Sale, M. J., and King, A. W.: A comparison of geographical information systems-based algorithms for computing the TOPMODEL topographic index, *Water Resources Research*, 40, W06303, 2004.

Quinn, P. F., Beven, K. J., and Lamb, R.: The  $\ln(a/\tan \beta)$  index: How to calculate it and how to use it within the topmodel framework, *Hydrological Processes*, 9, 161-182, 1995.

Stieglitz, M., Rind, D., Famiglietti, J., and Rosenzweig, C.: An Efficient Approach to Modeling the Topographic Control of Surface Hydrology for Regional and Global Climate Modeling, *Journal of Climate*, 10, 118-137, 1997.

Stocker, B. D., Spahni, R., and Joos, F.: DYPTOP: a cost-efficient TOPMODEL implementation to simulate sub-grid spatio-temporal dynamics of global wetlands and peatlands, *Geosci. Model Dev.*, 7, 3089-3110, 2014.

Zhu, X., Zhuang, Q., Lu, X., and Song, L.: Spatial scale-dependent land-atmospheric methane exchanges in the northern high latitudes from 1993 to 2004, *Biogeosciences*, 11, 1693-1704, 2014.

Zhuang, Q., Melillo, J. M., Kicklighter, D. W., Prinn, R. G., McGuire, A. D., Steudler, P. A., Felzer, B. S., and Hu, S.: Methane fluxes between terrestrial ecosystems and the atmosphere at northern high latitudes during the past century: A

retrospective analysis with a process-based biogeochemistry model, *Global Biogeochemical Cycles*, 18, GB3010 2004.

# 1 **Modeling spatiotemporal dynamics of global wetlands:** 2 **Comprehensive evaluation of a new sub-grid** 3 **TOPMODEL parameterization and uncertainties**

4  
5  
6 Zhen Zhang<sup>1,2,3</sup>, [Niklaus E. Zimmermann<sup>1</sup>](#), [Jed O. Kaplan<sup>4</sup>](#), [Benjamin Poulter<sup>2</sup>](#)

7 <sup>1</sup>[Dynamic Macroecology](#), Swiss Federal Research Institute WSL, Zürcherstrasse  
8 111, [8903](#) Birmensdorf, Switzerland

9 <sup>2</sup>Institute on Ecosystems and Department of Ecology, Montana State University,  
10 Bozeman, MT 59717, United States of America

11 <sup>3</sup>[Cold and Arid Regions Environmental and Engineering Research Institute](#),  
12 [Chinese Academy of Sciences, Lanzhou, 730000, Gansu, China](#)

13 <sup>4</sup>[Institute of Earth Surface Dynamics, University of Lausanne, 1015 Lausanne](#),  
14 [Switzerland](#)

15  
16 **Abstract:** Simulations of the spatiotemporal dynamics of wetlands are key to  
17 understanding the role of wetland biogeochemistry under past and future  
18 climate. Hydrologic inundation models, such as [TOPography-based hydrological](#)  
19 [model \(TOPMODEL\)](#), are based on a fundamental parameter known as the  
20 *compound topographic index (CTI)* and provide a computationally cost-efficient  
21 approach to simulate wetland dynamics at global scales. However, there remains  
22 large discrepancy in the implementations of TOPMODEL in land-surface models  
23 (LSMs) and thus their performance against observations. This study describes  
24 new improvements to TOPMODEL implementation and estimates of global  
25 wetland dynamics using the [LPJ-wsl \(“Lund-Potsdam-Jena WSL version”\)](#)  
26 [Dynamic Global Vegetation Model \(DGVM\)](#), and quantifies uncertainties by  
27 comparing three digital elevation model ([DEM](#)) products (HYDRO1k, GMTED,  
28 and HydroSHEDS) at different spatial resolution and accuracy on simulated  
29 inundation dynamics. In addition, we found that calibrating TOPMODEL with a  
30 benchmark wetland dataset can help to successfully delineate the seasonal and  
31 interannual variations of wetlands, as well as improve the spatial distribution of  
32 wetlands to be consistent with inventories. The HydroSHEDS DEM, using a river-  
33 basin scheme for aggregating the CTI, shows best accuracy for capturing the  
34 spatiotemporal dynamics of wetlands among the three DEM products. The  
35 estimate of global wetland potential/maximum is  $\sim 10.3 \text{ Mkm}^2$  ( $10^6 \text{ km}^2$ ), with a  
36 mean annual maximum of  $\sim 5.17 \text{ Mkm}^2$  for 1980-2010. [When integrated with](#)  
37 [wetland methane emission submodule, the uncertainty of global annual CH<sub>4</sub>](#)  
38 [emissions from topography inputs is estimated to be 29.0 Tg yr<sup>-1</sup>](#). This study  
39 demonstrates the feasibility of [TOPMODEL](#) to capture spatial heterogeneity of  
40 inundation [at large scale](#) and [highlights the significance of correcting maximum](#)

41 | [wetland extent to improve modeling of interannual variations in wetland areas](#).

42 | It additionally highlights the importance of an adequate investigation of  
43 | topographic indices for simulating global wetlands and shows the opportunity to  
44 | converge wetland estimates across LSMs by identifying the uncertainty  
45 | associated with existing wetland products.

46

47 | **Keywords:** Seasonal wetland dynamics, DGVM, LPJ, methane emission,  
48 | Topographic index, [Compound topography index \(CTI\)](#)

49

## 50 | **Introduction**

51 | For their ability to emit the greenhouse gas [methane \(CH<sub>4</sub>\)](#), wetland ecosystems  
52 | play a disproportionately important role in affecting the global climate system  
53 | through biogeochemical feedbacks (Fisher et al., 2011; Seneviratne et al., 2010).  
54 | Wetlands are thought to be the largest natural source of CH<sub>4</sub> emission by  
55 | contributing 20-40% of the total annual emissions to atmosphere, which adds a  
56 | strong radiative forcing from CH<sub>4</sub> (Bousquet et al., 2006; IPCC, 2013). The  
57 | seasonal and interannual distribution of wetland area remains one of the largest  
58 | uncertainties in the global CH<sub>4</sub> budget (Kirschke et al., 2013), in particular for the  
59 | roughly 60% of wetlands that are not inundated permanently (Petrescu et al.,  
60 | 2010). [Changes in the spatial extent of seasonally inundated](#) wetlands [was](#) most  
61 | likely a major driver for CH<sub>4</sub> variations during last glacial period (Kaplan, 2002)  
62 | and are considered as an important driver of the strong atmospheric CH<sub>4</sub> growth  
63 | rate resumed in 2007 (Nisbet et al., 2014) and in future climate change scenarios  
64 | (Stocker et al., 2013).

65

66 | Improving our understanding of the role of wetlands in global greenhouse-gas  
67 | (GHG) budgets requires a representation of wetlands and their biogeochemical  
68 | processes in land surface models (LSM) to both hindcast observed past  
69 | variations (Singarayer et al., 2011) and to predict future trajectories in  
70 | atmospheric CH<sub>4</sub> and terrestrial C balance (Ito and Inatomi, 2012; Meng et al.,  
71 | 2012; Spahni et al., 2011; Stocker et al., 2014; Zürcher et al., 2013). Dynamic  
72 | wetland schemes in LSMs were based on conceptual theories and physical  
73 | processes describing surface water processes (e.g., infiltration and  
74 | evapotranspiration) and water movement in the soil column using probability  
75 | distributions derived from subgrid topographic information (Beven and Kirkby,  
76 | 1979), or using analytical functional parametric forms with fixed parameters  
77 | (Liang et al., 1994). Currently, the most common approach for global wetland  
78 | modelling is to use a runoff simulation scheme such as TOPMODEL  
79 | (TOPography-based hydrological MODEL) (Beven and Kirkby, 1979; Kleinen et  
80 | al., 2012; Ringeval et al., 2012; Zhu et al., 2014), which includes the assumption  
81 | that lateral soil water transport driven by topography follows [the same](#)  
82 | [exponential decline as the vertical decrease in hydraulic conductivity](#) within soil  
83 | profiles in a basin (Sivapalan et al., 1987).

84  
85 TOPMODEL-based implementations have proven successful at capturing the  
86 broad geographic distribution of wetlands and their seasonal variability (Gedney  
87 and Cox, 2003; Ringeval et al., 2012; Stocker et al., 2014; Zhu et al., 2014), but  
88 have consistently overestimated [both](#) the extent [of wetlands](#) and duration of  
89 [inundation](#) at global and regional scale when compared with existing current  
90 surveys (Junk et al., 2011; Prigent et al., 2007; Quiquet et al., 2015). For instance,  
91 simulations using the Earth system model HadGEM2 predict much larger  
92 persistent Amazonian wetlands than [an](#) inventory (Collins et al., 2011). In  
93 general, independently determined wetland area using hydrologic modules of  
94 LSMs in The Wetland and Wetland CH<sub>4</sub> Inter-comparison of Models Projects  
95 (WETCHIMP) experiment simulated larger global wetland extent than those  
96 informed by remotely sensed product and inventories (Melton et al., 2013). This  
97 large disagreement also exists across specific regions (Ringeval et al., 2014). For  
98 example, Bohn et al. (2015) carried out a model inter-comparison of wetland  
99 extent on the West Siberian Lowland, one of the major wetland regions in high  
100 latitudes, and highlighted similar uncertainties of wetland extent simulation in  
101 the LSMs participating in the WETCHIMP experiment and using TOPMODEL.

102  
103 Meanwhile, uncertainties in wetland area estimation partly come from a paucity  
104 of observational datasets and different definitions of wetland (Matthews and  
105 Fung, 1987). Remotely sensed datasets have difficulties in capturing small or  
106 isolated water in saturated soils that are not flooded on the surface (Prigent et  
107 al., 2007), as well capturing the forested wetlands that obscure detection of  
108 inundation because of dense forest canopies (Bohn et al., 2015). In addition,  
109 ground-based survey or inventories that determine wetlands usually limited as  
110 static distribution that cannot provide temporal patterns for inundated area,  
111 making it hard to evaluate with simulated results. On the other hand, the  
112 definition of wetland for regional- or global-scale modelling assumes the land  
113 surface has both inundated and saturated conditions, which is not necessarily  
114 the same as inundated area measured by satellite observations (Melton et al.,  
115 2013).

116  
117 While prognostic wetland dynamics schemes are promising to resolve these  
118 observational issues, the configuration parameters for TOPMODEL are a  
119 potential source of uncertainty in estimating wetland dynamics (Marthews et al.,  
120 2015). [Among all parameters in TOPMODEL, the Compound Topographic Index](#)  
121 [\(CTI\) is of critical importance for determining inundated areas in terrain-related](#)  
122 [hydrological applications \(Ward and Robinson, 2000; Wilson and Gallant, 2000\).](#)  
123 [It measures the relative propensity for soils to become saturated \(Beven and](#)  
124 [Cloke, 2012\) and consequently it drives the accuracy of wetland area scaled to](#)  
125 [the larger grid cell \(Ducharne, 2009; Mulligan and Wainwright, 2013\). Although](#)  
126 [the importance of CTI has been highlighted, only few studies have so far](#)

127 | [evaluated the effect of CTI on modelling the spatial and temporal patterns of](#)  
128 | [global wetland dynamics. This is due to a limited availability of global CTI](#)  
129 | [products. During the last decade, the first CTI product at 1km resolution from](#)  
130 | [HYDRO1k global dataset released by U.S. Geological Survey \(USGS\) in 2000 has](#)  
131 | [become the most commonly applied global dataset for large-scale applications](#)  
132 | [\(Kleinen et al., 2012; Lei et al., 2014; Ringeval et al., 2012; Wania et al., 2013\).](#)  
133 | [However, HYDRO1k has been proven to potentially overestimate inundation](#)  
134 | [extent due to the quality of the underlying digital elevation model \(DEM\) \(Grabs](#)  
135 | [et al., 2009; Lin et al., 2010; Lin et al., 2013; Sørensen and Seibert, 2007;\).](#)  
136 | [With recent development of DEMs \(Danielson and Gesch, 2011; Lehner et al., 2008\),](#)  
137 | [there is a requirement to investigate uncertainties caused by CTI parameter.](#)

138  
139 | The primary goal of our study is to improve the modeling of dynamically varying  
140 | wetland extents with i) a parameter constraint to match integrated satellite and  
141 | inventory observations, and with ii) a better parameterizations of CTI values for  
142 | determining wetland seasonal cycles using new topographic data and  
143 | aggregation schemes (i.e., grid versus catchment). To this end, we develop a new  
144 | version of [Dynamic Global Vegetation Model \(DGVM\) LPJ-wsl \(“Lund-Potsdam-](#)  
145 | [Jena WSL version”\)](#) that includes the TOPMODEL approach for wetland extent  
146 | modelling by also accounting for soil thermal dynamics and high-latitude soil-  
147 | water freeze and thaw cycles, and by incorporating the necessary physical  
148 | processes ([e.g. snow aging](#)) that constrain global wetland dynamics. We utilize  
149 | three commonly used global DEM products to evaluate the effects of sub-grid  
150 | parameterizations on simulated global wetland extent uncertainties. We perform  
151 | six global simulations resulting from the combination of three DEM products and  
152 | two aggregation schemes under the same common experimental protocol. The  
153 | specific aims are: (1) to improve the performance of estimated wetland extent  
154 | based on TOPMODEL for the purpose of large-scale modelling, (2) to develop a  
155 | new parameterization scheme using inventory in combination with satellite-  
156 | based retrievals, and (3) to evaluate the uncertainties and the spatial and  
157 | temporal differences of CTI from three major DEM products in model behavior.

## 158 159 | **2 Model Descriptions and Experimental Design**

160 | The model LPJ-wsl is a process-based dynamic global vegetation model  
161 | developed for carbon cycle applications based on development of the LPJ-DGVM  
162 | (Sitch et al., 2003). LPJ-wsl includes land surface processes, such as water,  
163 | carbon fluxes, and vegetation dynamics that are intimately represented by plant  
164 | functional types (PFTs) (Poulter et al., 2011). The distribution of PFTs is  
165 | simulated based on a set of bioclimatic limits and by plant-specific parameters  
166 | that govern the competition for resources. The soil hydrology is modeled using  
167 | semi-empirical approach, with the soil treated as bucket consisting of two layers  
168 | each with fixed thickness (Gerten et al., 2004). The LPJ-wsl CH<sub>4</sub> model used in  
169 | this study is the same as presented in Hodson et al., (2011) and is a function of

170 two scaling factors ( $r_{CH_4:C}$  and  $f_{ecosys}$ ), soil temperature, soil-moisture-dependent  
171 fraction of heterotrophic respiration, and wetland extent according to the  
172 following equation:

$$173 \quad E(x, t) = r_{CH_4:C} \cdot f_{ecosys}(x) \cdot A(x, t) \cdot R_h(x, t) \quad (1)$$

174 where  $E(x, t)$  is wetland  $CH_4$  flux,  $A(x, t)$  is wetland extent,  $R_h(x, t)$  is  
175 heterotrophic respiration, [f<sub>ecosys</sub> is a scaling factor representing different wetland](#)  
176 [ecosystems, r<sub>CH<sub>4</sub>:C</sub> is the ratio C to CH<sub>4</sub> fluxes.](#)

177  
178 LPJ-wsl has been evaluated in previous studies using global inventory datasets  
179 and satellite observations and has been one of the participating models in the  
180 WETCHIMP study (Melton et al., 2013). Modifications [made here](#) to the original  
181 LPJ-wsl model and a detailed description of changes are summarized below:

182 - A permafrost module that simulate soil freeze and thaw processes, is  
183 implemented and modified following the Wania et al. (2009) study (see  
184 description in Sect. 2.1).

185 - The snow module from Wania et al. (2009) was included and modified to  
186 include some of the effects of snow ageing on snow thermal properties. We use  
187 an updated parameterization of soil thermal properties both for the permafrost  
188 and the snow module, which is calibrated by satellite observations specifically  
189 for global application.

190 - A new parameterization of soil texture was formulated based on the  
191 Harmonized World Soil Database (HWSD), which combines the recently  
192 collected extensive volumes of regional and national updates of soil parameter  
193 information (Nachtergaele et al., 2008). The new soil texture in LPJ-wsl follows  
194 the [U.S. Department of Agriculture](#) soil classification with 14 soil types grouped  
195 according to a particular range of particle-size fractions (e.g. sand, clay, loam,  
196 etc.), instead of using the original [Food and Agriculture Organization of the U.N.](#)  
197 classification with 9 soil types (Sitch et al., 2003). Thus, the volumetric water  
198 holding capacity, also defined as potential maximum soil water content (SWC), is  
199 assumed to vary spatially, calculated as a function of the surface soil texture  
200 using pedotransfer functions from Cosby et al., 1984. Wilting point, porosity,  
201 mineral soil content and organic soil content for each soil type are derived from  
202 a look-up table available from the [Air Force Weather Agency \(2002\)](#) as listed in  
203 Table 1.

204 The modified LPJ-wsl version is thus the starting point upon which the  
205 TOPMODEL-based wetland and permafrost modules are included (Sect. 2.2).

206

## 207 **2.1 Permafrost Model**

208 In order to consider the functional wetland area extension during the spring  
209 thaw and their shrinking or disappearances during autumn freeze, we added to  
210 LPJ-wsl a soil temperature scheme and freeze-thaw processes, as in Wania et al.  
211 (2009). The modified version considers the soil heat capacity and its thermal  
212 conductivity, which are both affected by the volumetric fractions of the soil

213 physical components, such as water-ice fraction, mineral soil, or peat. The  
 214 thermal scheme of LPJ-wsl is discretized vertically using 8-layers of variable  
 215 thickness, while the water-balance scheme is kept the same as the original LPJ-  
 216 DGVM, which means the daily changes in water content are allocated to the “old”  
 217 upper and lower layer of LPJ while considering percolation between these two  
 218 layers and baseflow from the lower layer. Fractional water and ice content in  
 219 each of the 8-layers is calculated on a daily time step. Soil temperature is  
 220 updated in the thermal routine and then passed to the hydrological routine to  
 221 determine the water-ice phase change in permafrost routine.

222

## 223 **2.2 Dynamic Wetland Model**

224 To represent the grid cell fraction covered by wetlands, we have implemented an  
 225 approach based on the TOPMODEL hydrological framework (Beven and Kirkby,  
 226 1979). TOPMODEL was initially developed to operate at the scale of large  
 227 watersheds using the channel network topography and dynamics contributing  
 228 areas for runoff generation, and was later extended to perform over areas that  
 229 are much larger than a typical river catchment (Gedney and Cox, 2003). The  
 230 fundamental information to determine the area fraction with soil water  
 231 saturation is derived from knowledge of the mean watershed water table depth  
 232 and a probability density function (PDF) of combined topographic and soil  
 233 properties (Sivapalan et al., 1987). The [CTI](#), which provides the sub-grid scale  
 234 topographic information in TOPMODEL, determines the likelihood of a grid box  
 235 to be inundated. It is defined as:

$$236 \quad \lambda_l = \ln\left(\frac{\alpha_l}{\tan\beta_l}\right) \quad (2)$$

237 where  $\lambda_l$  represents local CTI value,  $\alpha_l$  represent the contributing area per unit  
 238 contour,  $\tan\beta_l$ , the local topographic slope, approximates the local hydraulic  
 239 gradient where  $\beta$  is the local surface slope. The CTI distribution can be generated  
 240 from digital elevation models and near global datasets are readily available, e.g.  
 241 HYDRO1k dataset from USGS.

242

243 Following the central equations of TOPMODEL, the relationship between local  
 244 water table depth  $z_l$  and the grid mean water table depth  $z_m$  can be given as:

$$245 \quad \lambda_l - \lambda_m = f\{z_l - z_m\} \quad (3)$$

246 where  $\lambda_m$  is the mean CTI averaged over the grid box,  $f$  is the saturated  
 247 hydraulic conductivity decay factor with depth for each soil type. This equation  
 248 is valuable in that it relates the local moisture status to the grid box mean  
 249 moisture status based on the subgrid-scale variations in topography. Higher CTI  
 250 values than average are indicative of areas with higher water table depth than  
 251 average water table, and vice versa. We therefore calculate the inundated areas  
 252 ( $F_{wet}$ ) of all the sub-grid points within a grid cell that have a local water table  
 253 depth  $z_l \geq 0$ :

$$254 \quad F_{wet} = \int_{z_l}^{z_{max}} pdf(\lambda) d\lambda \quad (4)$$

255 where instead of using the CTI values themselves, we followed a common up-  
 256 scaling approach to approximate the distribution of CTI values within a grid cell  
 257 in order to reduce computation costs. Here, the discrete distribution of the CTI  
 258 for lowland pixels (i.e.  $\lambda_l \geq \lambda_m$ ) has been represented as an exponential function,  
 259 not as a three-parameter gamma distribution as applied in recent applications  
 260 for modeling wetland extent (Kleinen et al., 2012; Ringeval et al., 2012). As  
 261 shown in Figure 1, the new exponential function agrees well with the three-  
 262 parameter gamma distribution function when the CTI is larger than the mean  
 263 CTI  $\lambda_m$ . This change allows linking the inundated fraction directly to water table  
 264 depth, thus improving the parameterization by providing physical meaning and  
 265 fewer calibration parameters. This change also improves the parameterization of  
 266 fractional saturated area, especially in mountainous regions (Niu et al., 2005).

267

268 Finally, the wetland area fraction ( $F_{wet}$ ) is represented as:

$$269 \quad F_{wet} = F_{max} e^{-C_s f (\lambda_l - \lambda_m)} \quad (5)$$

270 Where  $C_s$  is a coefficient representing the topographic information [generated](#) by  
 271 fitting the exponential function to the discrete cumulative distribution function  
 272 (CDF) of the CTI.  $F_{max}$  is the maximum wetland fraction of a grid cell. Because of  
 273 the uncertainties involved in determining the water table depth, the hydraulic  
 274 factor  $f$ , and the coarse resolution DEMs, the maximum soil saturated fraction  
 275 calculated from discrete CDF are prone to large uncertainties and thus  
 276 complicate the comparison of the saturated fraction with existing observations  
 277 (Ducharne, 2009; Ringeval et al., 2012). Here, we introduce a [calibration of](#)  
 278 maximum wetland fractions  $F_{max}$ . We used the inventory-calibrated satellite  
 279 observations (see description in 3.3) combining with [inventory dataset](#) to  
 280 calculate representative long-term maximum wetland extents within each grid  
 281 box ( $0.5^\circ$ ), i.e. the parameter  $F_{max}$  for each grid cell i:

$$282 \quad F_{max_i} = \max(A_{GLWD_i}, \max(A_{SWAMP-GLWD_i})) \quad (6)$$

283  $A_{GLWD}$  represents wetland estimate from GLWD, and  $A_{SWAMP-GLWD}$  represents long-  
 284 term wetland estimate from SWAMPS-GLWD. The reason for combining these  
 285 two datasets is to take the advantage of satellite-based observations at capturing  
 286 temporal wetlands and inventory-based datasets at estimating forested wetlands  
 287 and small wetlands ignored by remote sensing. This [calibration](#) is also based on  
 288 the assumption that water is stagnant within local grids at large scale, in  
 289 particular for model using simple 'bucket' concept to calculate grid-mean water  
 290 table depth.

291 In addition, we used nonlinear least squares (nls) estimates to fit the [discrete](#)  
 292 CDF curve of CTI for lowlands ( $\lambda_l < \lambda_m$ ) to calculate parameter  $C_s$ , the parameter  
 293 that determines varying trend of wetland extent. By this, the parameters  
 294  $F_{max}$ ,  $\lambda_m$  and  $C_s$  for determining inundated areas are derived (Figure 2).

295

296 To account for the permafrost effects on soil infiltration properties, we followed  
 297 Fan and Miguez-Macho (2011) and Kleinen et al. (2012) who modified  $f$  by a

298 function  $k$  depending on January temperature  $T_{jan}$ . Since LPJ-wsl uses two soil  
 299 layers from the HWSD soil texture database ([Nachtergaele et al., 2008](#)) to  
 300 represent the different texture characteristics, the modification depends on the  
 301 combination of a look-up table (Table 1) from soil types and water table depth:

$$302 \quad k = \begin{cases} 1 & \forall T_{jan} > -5^{\circ}\text{C} \\ 1.075 + 0.015T_{jan} & -25^{\circ}\text{C} < \forall T_{jan} < -5^{\circ}\text{C} \\ 0.75 & \forall T_{jan} < -5^{\circ}\text{C} \end{cases} \quad (7)$$

303 Since the observed  $\text{CH}_4$  emission during winter are [mainly](#) attributed to physical  
 304 processes during soil freezing effects (Whalen and Reeburgh, 1992), for the  
 305 partially frozen wetland in high latitudes, we introduced an effective fraction of  
 306 wetland area ( $F_{wet}^{eff}$ ) defined by:

$$307 \quad F_{wet}^{eff} = \left( \frac{\omega_{liq}}{\omega_{liq} + \omega_{froz}} \right)_{50\text{ cm}} \cdot F_{wet} \quad (8)$$

308  
 309 where  $\omega_{liq}$  and  $\omega_{froz}$  are the fraction of liquid and frozen soil water content in  
 310 the upper soil (0-0.5 m) respectively. Since the liquid water content in the lower  
 311 soil layer gets trapped and cannot contribute to  $\text{CH}_4$  emission when upper soil is  
 312 frozen, we didn't consider the lower layer for surface wetland calculations.

313

### 314 **3 Experimental set-up and datasets**

#### 315 **3.1 Topographic information**

316 In this study we used three DEMs of varying spatial resolution, HYDRO1k [at 30](#)  
 317 [arc-second](#) (USGS, 2000; <http://lat.cr.usgs.gov/HYDRO1K>), Global Multi-  
 318 resolution Terrain Elevation Data 2010 (GMTED) [at 15 arc-second](#) (Danielson  
 319 and Gesch, 2011), and HydroSHEDS [at 15 arc-second](#) (Lehner et al., 2008) to  
 320 compare the effect of sub-grid topographic attributes on simulated seasonal and  
 321 interannual variability of wetlands. HYDRO1k, developed from the USGS released  
 322 30 arc-second digital elevation model of the world (GTOPO30), is the first  
 323 product that allowed spatially explicit hydrological routines applied in large-  
 324 scale applications (USGS, 2000). HydroSHEDS, developed from satellite-based  
 325 global mapping by the Shuttle Radar Topography Mission (SRTM), is a significant  
 326 improvement in the availability of high- resolution DEMs covering all land areas  
 327 south of  $60^{\circ}\text{N}$  (the limit of SRTM). For the areas at higher latitudes we used  
 328 HYDRO1k by aggregating the GTOPO30 DEM to provide global grids. GMTED was  
 329 produced using seven data sources including SRTM, global Digital Terrain  
 330 Elevation Data (DTED), Canadian elevation data, Spot 5 Reference3D data, and  
 331 data from the Ice, Cloud, and land Elevation Satellite (ICESat), covering nearly all  
 332 global terrain.

333

334 [To avoid mismatch of CTI value](#) inherent in computing CTI with different CTI  
 335 algorithms, we generated [three](#) global CTI maps based on the three DEM  
 336 products, instead of relying on existing CTI products [\(e.g. HYDRO1k CTI,](#)  
 337 [HydroSHEDS CTI product from Centre for Ecology and Hydrology\)](#) (Marthews et

338 al., 2015). Since studies show that multiple flow direction algorithms for  
339 calculating CTI give better accuracy compared with single-flow algorithms in flat  
340 areas (Kopecký and Čížková, 2010; Pan et al., 2004), thus we selected an  
341 algorithm from R library 'topmodel' (Buytaert, 2011), which applies the multiple  
342 flow routing algorithm of Quinn et al. (1995) to calculate the global CTI maps.  
343 The DEMs from HYDRO1k and HydroSHEDS had been previously processed for  
344 hydrological-correction, meaning that the DEMs were processed to remove  
345 elevation depressions that would cause local hydrologic 'sinks'. To include a  
346 comparison of (hydrologically) corrected and uncorrected DEMs in our analyses  
347 as some studies have been done previously (Stocker et al., 2014), the GMTED  
348 DEM [was applied](#) without hydrological correction.

349

### 350 **3.2 Description of the simulation**

351 For running LPJ-wsl with permafrost and TOPMODEL, we used global  
352 meteorological forcing (temperature, cloud cover, precipitation and wet days) as  
353 provided by the Climatic Research Unit (CRU TS 3.22) at 0.5° resolution (Harris  
354 et al., 2014). To spin up the LPJ-wsl model using the CRU climatology, climate  
355 data for 12-months were randomly selected from 1901-1930 and repeated for  
356 1000 years with a fixed pre-industrial atmospheric CO<sub>2</sub> concentration. The first  
357 spinup simulation started from initial soil temperature derived from LPJ-wsl  
358 simulated results on January 1901 and continued with a land use spin-up  
359 simulation. These procedures ensure that carbon stocks and permafrost are in  
360 equilibrium before performing transient simulations. The transient simulations,  
361 with observed climate and CO<sub>2</sub> were performed with monthly climate  
362 disaggregated to daily time steps over the 1901-2013 period. The 1993-2013  
363 years were used for evaluation against satellite data and inventories.

364 [One of key assumptions in TOPMODEL is that the water table is recharged at a](#)  
365 [spatially uniform and steady rate with respect to the flow response timescale of](#)  
366 [the catchment \(Stieglitz et al., 1997\). Given the fact that we consider the water to](#)  
367 [be stagnant within each grid, the mean CTI parameter was estimated with two](#)  
368 [alternative schemes: \(1\) a regular 'grid-based' or gridded approach, i.e., the](#)  
369 [subgrid CTI values were averaged per 0.5° grids, and \(2\) an irregular 'basin-](#)  
370 [based' approach, where mean CTI were calculated over the entire catchment](#)  
371 [area in which the respective pixel is located. For generating a global catchment](#)  
372 [map at 0.5° resolution, we applied a majority algorithm in the case of multi-](#)  
373 [catchments in a grid with consideration of avoiding isolated pixels for specific](#)  
374 [river basin. There are two catchment area products applied in this study,](#)  
375 [HYDRO1k \(2013\) and HydroSHEDS. Similarly, the parameter  \$C\_s\$  was generated](#)  
376 [using nonlinear least squares estimates from both of these two different CTI](#)  
377 [calculation strategies. Two sets of model experiments were carried out to](#)  
378 [compare the wetland dynamics under basin and grid-based TOPMODEL](#)  
379 [parameterizations respectively \(Table 2\).](#)

380

### 381 3.3 Evaluation and benchmarking data

382 Since the soil freeze-thaw cycles are a key component for determining seasonal  
383 cycles of wetlands in cold regions, in this study we benchmarked the general  
384 pattern of permafrost locations by comparing the model output against satellite  
385 observations of freeze and thaw status and inventories of permafrost extent.  
386 Since soil depth in LPJ-wsl is held at 2.0 m for the permafrost module, the  
387 permafrost extent in this study is defined as the lower soil (0.5-2 m) that is  
388 always at or below the freezing point of water 0°C for multiple years. The  
389 permafrost extent map at 0.5-degree resolution from National Snow and Ice Data  
390 Center (NSIDC) is adopted for benchmarking (Brown et al., 2001). The global  
391 dataset of Freeze/Thaw (FT) status is derived from satellite microwave remote  
392 sensing provided by the Numerical Terradynamic Simulation Group (NTSG) at  
393 University of Montana and is based on daily maps over a 34-year record (1979-  
394 2012). It represents the FT status of the composite landscape vegetation-snow-  
395 soil medium to constrain surface water mobility and land-atmosphere carbon  
396 fluxes (Kim et al., 2012).

397  
398 Two global inundation products derived from satellite observations were  
399 additionally used for evaluation purposes: the Global Inundation Extent from  
400 Multi-Satellites (GIEMS), derived from visible (AVHRR) and active (SSM/I) and  
401 passive (ERS) microwave sensors over the period 1993-2007; the Surface Water  
402 Microwave Product Series (SWAMPS), derived from active (SeaWinds-on-  
403 QuikSCAT, ERS, and ASCAT) and passive (SSM/I, SSMI/S, AMSR-E) microwave  
404 sensors over the period 1992-2013. This new SWAMPS global dataset, hereby  
405 denoted as SWAMPS-GLWD, was first developed at NASA JPL (Schroeder et al., In  
406 preparation). We re-scaled this dataset with the Global Lake and Wetland  
407 Database (GLWD) (Lehner and Döll, 2004), a well-established global inventory of  
408 water bodies at high resolution to match SWAMPS-GLWD with the inventory  
409 estimates. This post-processed SWAMPS product covers the required regions for  
410 forested wetlands, which are not readily observable by passive or active  
411 microwave measurements (Poulter, [et al., In preparation](#)). For evaluating  
412 regional wetland patterns, we selected two study areas (the largest peatland  
413 West Siberian Lowland (WSL); the largest floodplain, Amazon River Basin).  
414 Three wetland map products over the WSL from (Sheng et al., 2004), (Peregon et  
415 al., 2008) and (Tarnocai et al., 2009) (denoted by “Sheng2004”, “Peregon2008”,  
416 Tarnocai2009 respectively) and one up-date high resolution dual-season  
417 inundated area inventory for lowland Amazon basin from [Japanese Earth](#)  
418 [Resources Satellite \(JERS-1\) were applied](#) (Hess et al., 2015) (denoted by  
419 [“Hess2015”](#)). We aggregated all above-mentioned datasets from the native 25  
420 km to a 0.5-degree spatial resolution and from daily to monthly temporal  
421 resolution for comparison with model outputs (Table A1).

422

## 423 4 Results

#### 424 4.1 Evaluation against observations

425 We first evaluated the permafrost module that constrains the seasonal cycles of  
426 wetland area in cold regions with respect to inventory and remote sensing  
427 observations. Figure\_3a compares the spatial distribution of permafrost extent  
428 from inventory and the modeled permafrost extent over the period 1980-2000.  
429 Figure 3b gives the spatial distribution of Spearman rank correlation between  
430 the simulated and observed number of monthly frozen-days. The modeled  
431 permafrost extent shows high agreement with benchmarking dataset, with a  
432 slightly higher coverage of permafrost regions in North-Western Eurasia. The  
433 model successfully captures the seasonally frozen soil, which is closely linked to  
434 surface wetland formation and seasonal variation of wetland in cold regions.  
435 Most of the regions reveal a temporal correlation  $> 0.9$ , while Eastern Siberia and  
436 the Southern permafrost distribution edge is generally around 0.5. The lower  
437 correlation in East Siberia probably originates from two issues: high snow [depth](#)  
438 in LPJ-wsl that insulates soil temperature and [consequent delay of soil](#)  
439 [temperature to reach](#) complete freezing; and the relatively large uncertainty of  
440 FT-ESDR derived soil frozen status in those regions (Kim et al., 2012). This  
441 difference can be partly explained by the different representation of frozen  
442 status between simulated results and satellite retrievals. Remotely sensed maps  
443 reflect the mixed condition of the upper vegetation canopy, snow layer and  
444 surface soil, while the simulated frozen days only represent the frozen state of  
445 topsoil.

446  
447 Figure 4 illustrates the model evaluation at the regional scale over the West  
448 Siberian Lowland (Figure 4). The model generally captures the spatial extent of  
449 the seasonal maximum wetland area fraction across the whole WSL for the JJA  
450 season successfully. However, the TOPMODEL approach without calibration  
451 (denoted as 'Original') shows large areas with relatively low wetland proportion  
452 and cannot capture high values. This suggests poor model performance in  
453 simulating wetland areas without  $F_{max}$  calibration. The calibrated model  
454 generally exhibits good agreement with inventories and satellite retrievals. It is  
455 especially successful at capturing the spatial heterogeneity of wetland areal  
456 extent over the whole WSL regions. LPJ-wsl simulated results reveal additional  
457 wetland area in the northeast, where wetlands entirely lacked in the GLWD map,  
458 although captured in other datasets. Meanwhile, LPJ-wsl captured the higher  
459 wetland area in region between 61 and 66°N and 70 and 80°E regions compared  
460 with GLWD, where mire/bog/fen was dominated across that region. LPJ-wsl also  
461 maintained well the spatial pattern of wetlands in forested region south of 60°N,  
462 which was captured by inventories (Sheng2004, Peregona2008, and GLWD), but  
463 was missed by two satellite products (SWAMPS-GLWD, GIEMS) due to the  
464 limitation of remotely sensed datasets in detecting water under vegetative  
465 canopy and/or due to reduced sensitivity.

466 As illustrated in Figure 5, LPJ-wsl captured the spatial pattern of simulated  
467 wetlands well with lower estimates of the total wetland area in low-water season  
468 compared to the JERS-1 observed maps. Differences between Hess2015 and LPJ-  
469 wsl maps were primarily in two regions, Marañon-Ucayali region of Peru (MUP,  
470 3-7°S, 73-77°W) and Llanos de Moxos in Bolivia (LMB, 11-17°S, 60-68°W). LPJ-  
471 wsl shows higher wetland coverage in MUP while Hess2015 indicates high  
472 wetland fraction in LMB in high-water season. Global satellite products largely  
473 ignore the LMB region that was partly captured in LPJ-wsl, indicating that LPJ-  
474 wsl using hybrid TOPMODEL approach can yield estimates closer to those of  
475 fine-resolution mapping, while large-scale satellite products are likely to  
476 underestimate Amazon wetland extent because of their coarse spatial resolution  
477 that limit the ability to detect inundation outside of large wetlands and river  
478 floodplains (Hess et al., 2015).

479 | [To evaluate the effect of  \$F\_{max}\$  calibration](#) on CH<sub>4</sub> emission estimates, two  
480 | estimates of CH<sub>4</sub> ([with and w/o calibration](#)) over the WSL regions were  
481 | compared with observation-based estimate from Glagolev et al. (2011) (Figure  
482 | 6). The 3-year mean annual total emission from [original version](#) is  $6.29 \pm 0.51$  Tg  
483 | CH<sub>4</sub> yr<sup>-1</sup>, falling into the upper part of range from land surface models and  
484 | inversions (Bohn et al., 2015), [whereas](#) the calibrated version is close to the  
485 | estimate of Glagolev et al. (2011) ( $3.91 \pm 1.29$  Tg CH<sub>4</sub> yr<sup>-1</sup>) [with  \$4.6 \pm 0.45\$  Tg CH<sub>4</sub>](#)  
486 | [yr<sup>-1</sup>](#). In addition, [the spatial pattern of CH<sub>4</sub> emission with  \$F\_{max}\$  calibration shows](#)  
487 | [better agreement with observation than non-calibration one](#) with relatively  
488 | [larger](#) emissions in Taiga forests [and](#) central region (55-65°N, 65-85°E). We also  
489 | compared our estimates with recent airborne [campaign](#) observations for Alaska  
490 | during 2012 [growing seasons](#). [Estimates with  \$F\_{max}\$  calibration](#) also falls well into  
491 | the range of recent estimate ( $2.1 \pm 0.5$  Tg CH<sub>4</sub> yr<sup>-1</sup>) for Alaska based on airborne  
492 | observations (Chang et al., 2014) with a total of 1.7 Tg CH<sub>4</sub> yr<sup>-1</sup> during 2012  
493 | growing season ( $3.1$  Tg CH<sub>4</sub> yr<sup>-1</sup> from non-calibrated estimate), indicating  
494 | [necessity](#) of  [\$F\_{max}\$  calibration](#) to accurately capture annual CH<sub>4</sub> emission and  
495 | spatial variability for boreal wetlands.

## 496 **4.2 Spatial distribution**

497 Several observations applicable to evaluate the difference among sub-grid  
498 parameterizations of TOPMODEL are available for the WSL region. Figure 7 lists  
499 | the spatial patterns of simulated JJA ([June-July-August](#)) wetland area over WSL  
500 regions to illustrate differences among wetland maps. The general patterns of  
501 wetland extent are substantially similar, because they both used the same  
502 calibrated  $F_{max}$  map. Both of these datasets show wetlands distributed across  
503 most of the WSL, with extensive wetlands in the central region (55-65°N, 60-  
504 90°E). However, the detailed pattern is differing between the approaches and  
505 DEMs used, which indicate the uncertainty of parameterizations on wetland  
506 distribution. The basin-based parameterization can capture the higher wetland  
507 areas in regions with bog, mire, or fen vegetation in the central east (63-67°N,  
508 | 85-90°E) as was found in the GLWD benchmark map. The [grid](#)-based

509 | parameterizations fail to reproduce this pattern. It seems that the [grid](#)-based  
510 | parameterizations are less [sensible](#) in capturing the spatial heterogeneity  
511 | throughout most of the WSL. The difference in parameterization derived from  
512 | DEM datasets also affects the simulated regional pattern. Both of HydroSHEDS-  
513 | based results successfully reproduce the high wetland fractions in the southern-  
514 | forested regions (55-60°N, 65-80°E), while HYDRO1k and GMTED both cannot  
515 | capture this feature. Note that GMTED [is](#) derived from the same DEM product  
516 | SRTM [as HydroSHEDS but without hydro-correction](#), indicating the importance  
517 | of hydro-correction in simulating spatial patterns of wetlands.

518

519 | The comparison of simulated mean annual minimum, maximum, and amplitude  
520 | of wetland extent with observational datasets (Table 3) reveals that the  
521 | simulated wetland area for 1980-2010 falls within the range of  $4.37 \pm 0.99$  Mkm<sup>2</sup>  
522 | (Mkm<sup>2</sup>=10<sup>6</sup> km<sup>2</sup>). This number is close to GIEMS (5.66 Mkm<sup>2</sup>) (Prigent et al.,  
523 | 2012) and inventory-based estimates (6.2 Mkm<sup>2</sup>) (Bergamaschi et al., 2007)  
524 | after exclusion of other water bodies like lakes, rivers, and rice paddies (Leff et  
525 | al., 2004). Considering potential underestimation of satellite-based observation  
526 | in forested regions, the realistic estimate could possibly be in the upper part of  
527 | our range. Note that one must be careful when [directly](#) comparing model results  
528 | with the observational datasets based on inventories or digitized maps, because  
529 | these datasets might represent the long-term maximal area as wetland potential.  
530 | The higher seasonal wetland extent in GIEMS compared with LPJ-wsl could be  
531 | partly due to permanent wetlands that [are hard to detect by GIEMS](#). Lastly, the  
532 | definition of wetland is another possible source of discrepancy. Remotely sensed  
533 | inundation datasets [emphasizes on open water](#) while wetland area in our study  
534 | is specifically defined from inventories following the National Wetlands Working  
535 | Group (1988) classification that include peatlands, mineral wetlands, and  
536 | [seasonally inundated](#) shallow waters.

537

### 538 | **4.3 Seasonal cycle**

539 | The shapes of the seasonal patterns in wetland area are generally similar in  
540 | model simulation compared to satellite observations, despite disagreement in  
541 | the timing of the seasonal cycle of wetland area in some boreal regions (Figure  
542 | 8). The modeled results show slightly larger wetland areas in the [SON \(Sept-Nov\)](#)  
543 | [months](#) than satellite-based observations. The [larger](#) seasonal wetland areas  
544 | during SON may originate from the longer [periods of unfrozen and relatively](#)  
545 | [water saturated soil in the model data](#). It thus seems realistic that the satellite-  
546 | based inundation product AMSR-E observed a similar trend of seasonal  
547 | inundation patterns for North America and Boreal Eurasia (Jennifer et al., 2014).  
548 | This is also supported by field studies in boreal regions, indicating that water  
549 | table depth during the SON [months](#) is still in a high level and soil temperature is  
550 | above freezing status (Rinne et al., 2007; Turetsky et al., 2014). In contrast, the  
551 | modeled seasonal cycle of wetland in tropical and temperate regions show a

552 good agreement with GIEMS and SWAMPS-GLWD. Given the difficulties of  
553 satellite-based observations in detecting wetlands in forested regions and the  
554 reduced sensitivity where open water fraction is low (<10%) (Prigent et al.,  
555 | 2007), the inundation numbers by GIEMS might slightly underestimate the area  
556 compared with the simulated results.

557

558 | Figure 8 reveals that the six [data sets of monthly wetland extent for 1993-2007](#)  
559 | [based](#) on different [TOPMODEL parameterization](#) show the same general  
560 behavior in the different regions. The six data sets are highly correlated, with  
561 largest differences at the maximal wetland extents during growing seasons,  
562 especially in the boreal regions. In addition, the differences in seasonal cycle  
563 among the six model experiments are relatively small, mostly below 5%  
564 regardless of the month. This indicates that the averaged total wetland area is  
565 not dependent on the introduction of the new sub-grid parameterizations at the  
566 global scale. Among the DEM datasets, HYDRO1k shows the largest difference  
567 | between basin and [grid](#)-based estimates with annual mean wetland area of  
568 89,663 km<sup>2</sup> in boreal regions, while HydroSHEDS has a lowest difference of 6550  
569 km<sup>2</sup> between the two versions. Examining the seasonal amplitude for basin-  
570 based schemes, HydroSHEDS shows a better agreement with satellite-based  
571 observations than the other two datasets.

572

#### 573 **4.4 Interannual variability**

574 For evaluating the performance of all the sub-grid parameterizations, we  
575 | calculated [the](#) Pearson's correlation coefficient (r) between modeled and  
576 | satellite-based results (Table 4). Generally, the comparison demonstrates that  
577 simulated interannual variability shows a good agreement with GIEMS and  
578 | SWAMPS-GLWD in most regions [as defined in Fig. 2](#). For boreal and tropical  
579 regions, all correlation coefficients are ranging from 0.7-0.8. The comparison of  
580 the inter-annual trends (Figure A1) indicates that absolute values of simulated  
581 interannual variations are close to satellite-based observation with good  
582 agreement in shape and timing in these regions. This demonstrates the ability of  
583 TOPMODEL to capture the large-scale variations in wetland/inundation. Highest  
584 disagreements are found in temperate regions that are strongly affected by  
585 human activities (likely strong global anthropogenic effect on continental surface  
586 freshwater), which is indicated by GIEMS (Prigent et al., 2012) but not by  
587 modeled results.

588

589 The interannual variability originating from six different sub-grid DEM  
590 parameterizations is very similar between these schemes with Spearman rank  
591 correlation coefficient  $r > 90\%$ . Among the six schemes, the parameters  
592 calculated from HydroSHEDS using basin-based statistics result in better  
593 agreement between simulated and measured wetland area than the other  
594 schemes. In most regions, the SWAMPS-GLWD and GIEMS are consistent in their

595 observed wetland area patterns, except for temperate regions (e.g. Temperate  
596 South America, Temperate North America, Europe). This confirms that the  
597 differences in surface water extent detection between GIEMS and SWAMPS-  
598 GLWD, which might be caused by observational behaviors from different satellite  
599 instruments and algorithms. In addition, parameters estimation based on river  
600 basins are slightly better than [grid](#)-based results.

601

## 602 **5.Discussion**

### 603 **5.1 Wetland modelling based on TOPMODEL concept**

604 The coupling between LPJ-wsl and TOPMODEL with [calibrated parameters](#) as  
605 described in this study, [improves the dynamical simulation of wetlands, in](#)  
606 [particular their geographic location and extent](#). This is based on the recent  
607 discussions of the suitability of TOPMODEL applications to simulate wetland  
608 variations at large spatial scale (Ringeval et al., 2012), and intercomparisons of  
609 the wetland-area-driven model bias in CH<sub>4</sub> emission at regional scale (Bohn et  
610 al., 2015). The [large discrepancies of wetland area among LSMs](#) so far have  
611 shown extensive disagreement with inventories and remotely sensed inundation  
612 datasets (Melton et al., 2013), [which is](#) partly due to large varieties of schemes  
613 used for representing hydrological processes, [or](#) due to the inappropriate  
614 parameterizations for simulating inundations. [Our results suggest that](#)  
615 [benchmarking  \$F\_{max}\$](#)  is necessary for global wetland modelling.

616

617 The simulation of hydrological dynamics within LSMs remains relatively simple  
618 because the [physical processes described in LSMs](#) occur at much finer spatial  
619 scales (Ducharne, 2009; Mulligan and Wainwright, 2013). The coupling of  
620 TOPMODEL with process-based LSMs allows [the retrieval of the maximum](#)  
621 saturated fraction ( $F_{max}$ ), which is defined by the pixels with no water deficit  
622 estimated from the partial integration of the spatial distribution of CTI in a  
623 catchment. [The](#) estimated distribution of  $F_{max}$  is much larger than that obtained  
624 from the satellite-based observations (Papa et al., 2010). As a key parameter for  
625 determining the soil saturated area, the calculation of  $F_{max}$  at large scale is prone  
626 to large uncertainties, in particular linked to uncertainties in topographic  
627 information, as well as the hydrological processes implemented in large-scale  
628 LSMs. Ringeval et al. (2012) pointed to the difficulty of two-layer bucket  
629 hydrological model in estimating the mean deficit to the saturation over each  
630 grid-cell. This can lead to nonrealistic absolute values of the contributing area in  
631 a watershed. We constructed several strategies for optimizing  $F_{max}$  by correcting  
632 topographic information to match the wetland inventories (Gedney and Cox,  
633 2003; Kleinen et al., 2012). This is one possible solution for global wetland  
634 modeling as it assumes that wetland area can be considered constant at coarse  
635 spatial resolution (e.g. 0.5° or 1°), following the classical approach of Beven and  
636 Kirkby (1979). However, due to the uncertainties from topographic information  
637 used in global applications and due to limitations in model parameterizations,

638 | this approximation cannot capture the fine\_scale wetland extent, which  
639 | [complicates the comparison to inventories.](#)

640

641 | [Integration of satellite-based and inventory-based observations to calibrate  \$F\_{max}\$](#)   
642 | [is highlighted in this study. Combining SWAMPS and GLWD led to simulated](#)  
643 | [wetland area consistent with detailed regional distribution \(Poulter et al., in](#)  
644 | [preparation\). Our estimation of global wetland potential/maximum is ~ 10.3](#)  
645 | [Mkm<sup>2</sup>, and in agreement with](#) the deduction (10.4 Mkm<sup>2</sup>) from recent estimates  
646 | at finer resolution for total open water (~17.3 Mkm<sup>2</sup>) (Fluet-Chouinard et al.,  
647 | 2015), lakes (~5 Mkm<sup>2</sup>) (Verpoorter et al., 2014), and rice paddies (1.9 Mkm<sup>2</sup>)  
648 | (Leff et al., 2004). [The calibration of  \$F\_{max}\$  maintains capability of simulating the](#)  
649 | [wetland dynamics on decade-to-century long time scales. As shown in Figure 9,](#)  
650 | [the wetland potential for permafrost and arid/semi-arid regions is high. Even in](#)  
651 | [tropical regions, there is ~ 20-30% of potential areas can be inundated.](#)

652

653 | According to our evaluation using satellite-based observations and inventories,  
654 | the spatial distribution of the wetland areas and its temporal variability are  
655 | generally well captured by our model, both at regional and global scales. In  
656 | addition, the modeled wetland areas and interannual variability compare well  
657 | with inventories and satellite-based observations respectively. Unfortunately,  
658 | the wide disagreement in simulated wetland dynamics among estimates from  
659 | WETCHIMP hampers our ability to assess model performance (Bohn et al.,  
660 | 2015). Narrowing down the uncertainty of wetland areas by existing maps could  
661 | minimize the controversial use of the definition between wetlands and  
662 | inundations. Wetlands have considerable variations in hydrologic conditions,  
663 | size, locations that make [difficult](#) to [reconcile a single definitions of wetlands.](#) In  
664 | current parameterizations, the connectivity of wetlands cannot be represented  
665 | since wetlands are considered invariant within grid cells.

666

## 667 | **5.2 CTI parameterizations**

668 | As shown in this study, global wetland simulations can benefit from improved  
669 | spatial resolution of topographic maps, thus creating [a](#) more realistic  
670 | representation of processes at sub-grid resolution, and correspondingly better  
671 | inundation simulations. This is [supporting](#) the ideas of Wood et al. (2011) who  
672 | claimed that higher-resolution modeling leads to better spatial representation of  
673 | saturated and nonsaturated areas, even though limitations in up-scaling  
674 | parameterizations may potentially outrun this advantage. The comparison  
675 | between HydroSHEDS and GMTED also indicated that, for capturing inundated  
676 | areas under the same spatial resolution, the parameter maps derived from DEM  
677 | without hydrological corrections have less accuracy compared to corrected ones  
678 | (Lehner and Grill, 2013). Without hydrological corrections, valleys would appear  
679 | as closed depressions in the DEM, leading to an underestimation of inundated  
680 | areas (Marthews et al., 2015). It could be foreseen that if DEMs in process-based

681 models are being applied at higher resolution, this drawback could be amplified.  
682 The comparison between basin- and [grid](#)-based parameterizations suggests that  
683 [grid](#)-based calculations are not appropriate and consequently underestimates  
684 wetland areas even when assuming invariant inundated areas at large scale.

685  
686 [The algorithm to calculate CTI is another potential source of error for modelling](#)  
687 [inundations. The method we applied here is based on calculating a CTI](#)  
688 [distribution map using a simple algorithm in the R package 'topmodel' instead of](#)  
689 [using an existing CTI product with improved contributing area. The algorithm](#)  
690 [we applied using the multi-flow direction algorithm that allows for multiple in-](#)  
691 [flow and out-flow of water among neighboring pixels when generating](#)  
692 [topographic values. This could potentially overestimate the contributing areas](#)  
693 [\(Pan et al., 2004\). As a result, it might underestimate the wetland areas within](#)  
694 [each grid cell, and slightly underestimate the temporal pattern of saturated areas](#)  
695 [because of improper estimates of parameter  \$C\_s\$  \(Güntner et al., 2004\). One](#)  
696 [limitation of HydroSHEDS is that its projection is not equal-area like HYDRO1k](#)  
697 [\(Marthews et al., 2015\), and will cause a potential bias in slope calculation along](#)  
698 [east-west directions at high latitudes. However, since there is no common](#)  
699 [method to calculate slope or flow direction, we believe that our calculations](#)  
700 [provide a reasonable approximation for global applications.](#)

701  
702 [In addition, TOPMODEL parameterizations have considerable influence on](#)  
703 [simulated  \$CH\_4\$  fluxes that the uncertainty of mean annual  \$CH\_4\$  emissions from](#)  
704 [topography inputs is estimated to be  \$29.0 \text{ Tg yr}^{-1}\$  \(Table 5\). All of the model](#)  
705 [estimates generally fall within the range of inversion estimates. The differences](#)  
706 [of  \$CH\_4\$  emissions among the model experiments is related to simulated](#)  
707 [magnitude of wetland extents because the fraction of  \$CH\_4\$  emissions from tropics](#)  
708 [\( \$\sim 63\%\$ \) and Extratropics \( \$\sim 27\%\$ \) keep constant due to same parameters  \$r\_{C:CH\_4}\$](#)   
709 [and  \$f\_{ecosys}\$ . The importance of hydrological correction is highlighted by results](#)  
710 [based on GMTED, suggesting that applying topography map without hydro-](#)  
711 [correction may potentially underestimate  \$CH\_4\$  fluxes due to lower hydrological](#)  
712 [connectivity that dampen generating of inundation. In addition, fine-scale](#)  
713 [topography data like HydroSHEDS shows higher  \$CH\_4\$  fluxes than HYDRO1k,](#)  
714 [suggesting its influence on capturing small wetlands/inundated areas that may](#)  
715 [be ignored by coarse-resolution products.](#)

716

717

### 718 **5.3 Future needs for global wetland modelling**

719 Substantial progress has been made in the development of wetland modeling,  
720 but the wide disagreement among estimates from LSMs still exists (Bohn et al.,  
721 2015; Melton et al., 2013). Considering that spatiotemporal variation of wetland  
722 area can largely influence  $CH_4$  emissions, the selection of appropriate maps  
723 needs to be done with care. The parameterization and evaluation of multi-  
724 resolution topographic products presented in this study would enhance global  
725 wetland modeling if progress could be made in four areas particularly:

726 • *Improved parameters of TOPMODEL for large-scale application.* Our results  
727 demonstrate that model simulation after calibrating TOPMODEL are  
728 comparable in absolute value with inventories and satellite-based  
729 observations at coarser resolution. This supports the ideas of (Beven and  
730 Cloke, 2012) that an appropriate scale-dependent subgrid  
731 parameterization is the main challenge, regardless of whether it is carried  
732 out at global modeling scales or landscape scales. The saturated soil water  
733 content is the decisive unit that determines wetland distributions and  
734 reasonable estimates of global wetland areas. Hydraulic parameters,  
735 which describe soil characteristics for water movement, are critical for  
736 modelling wetland seasonal cycles (Marthews et al., 2014). Assessing the  
737 uncertainties introduced by aggregating sub-pixel to pixel areas also need  
738 to be evaluated.

739 • *Implementing human impact within wetland modeling.* There are  
740 evidences from long-term satellite-based observations detecting a  
741 significant effect of human activities on wetland drainage at continental  
742 scale (Prigent et al., 2012). At finer scale, the variability of wetland extent  
743 has also been affected by land-use change (e.g. wetland restoration,  
744 deforestation, drainage for forestry, agriculture, or peat mining) and  
745 consequently influences spatiotemporal patterns of CH<sub>4</sub> emission  
746 (Petrescu et al., 2015; Zona et al., 2009). Land-use change may therefore  
747 feedback water available to wetlands through altering water balance  
748 between land surface and atmosphere (Woodward et al., 2014). An  
749 implementation of human impacts within LSMs at large scale may be  
750 important for accurate estimation of interannual variations of wetlands.

751 • *Improved modelling of soil moisture.* The quality of soil moisture  
752 simulation using LSMs depends largely on the accuracy of the  
753 meteorological forcing data, surface-atmosphere interaction schemes, and  
754 a wide range of parameters (Zhang et al., 2013) (e.g. CO<sub>2</sub> concentration,  
755 albedo, minimum stomatal resistance, and soil hydraulic properties). As  
756 the fundamental variable for determining water table depth at global  
757 scale (Fan et al., 2013), soil moisture plays a key role in simulating the  
758 spatiotemporal variability of wetland dynamics. Since it is impossible to  
759 produce accurate large-scale estimates of soil moisture from in situ  
760 measurement networks (Bindlish et al., 2008; Dorigo et al., 2011),  
761 simulation combined with long-term surface and root zone remotely  
762 sensed estimates (de Rosnay et al., 2013; Kerr et al., 2010) via data  
763 assimilation technology, represents a strategy to improve the capturing of  
764 global wetland variability. Future hydrology-oriented satellite missions  
765 such as Soil Moisture Active Passive (SMAP) (Entekhabi et al., 2010), and  
766 Surface Water and Ocean Topography (SWOT) mission (Durand et al.,  
767 2010) are expected to provide soil moisture and will improve the capacity  
768 of global soil moisture simulations.

769 • *Improved satellite benchmark observations.* Current satellite-based  
770 estimates of wetland area remain generally uncertain, despite being  
771 important for monitoring global wetland variability. Remotely sensed  
772 global inundation [is](#) prone to underestimate [small](#) wetlands, as well as  
773 covered with dense vegetation canopies (Papa et al., 2010). Moreover,  
774 estimated coastal areas show large bias due to interference with the  
775 ocean surface (Prigent et al., 2007). This raises [the need](#) for benchmark  
776 dataset [useful](#) to generate accurate products with lower uncertainties.  
777 Downscaling methodology has been made to refine existing satellite-  
778 based inundation estimates by coupling the mapping process with  
779 reliable inventories (Fluet-Chouinard et al., 2015). This may improve  
780 global inundation products, as well as the TOPMODEL parameter  
781 estimation in the future.

782

### 783 **Conclusion**

784 The new LPJ-wsl version incorporates a TOPMODEL approach and a permafrost  
785 module representing soil freeze-thaw processes to simulate global wetland  
786 dynamics. Once the  $F_{max}$  parameter in TOPMODEL was calibrated against a  
787 benchmark dataset, the model successfully mapped regional spatial pattern of  
788 wetlands in West Siberian Lowland and lowland Amazon basin, and captured  
789 [well](#) the spatiotemporal variations of global wetlands. The parameterization of  
790 TOPMODEL based on three DEM products, HYDRO1k, GMTED, and HydroSHEDS  
791 revealed that HydroSHEDS performed best in capturing the spatial heterogeneity  
792 and interannual variability of inundated areas compared to inventories. River-  
793 basin based parameterization schemes using HYDRO1k and GMTED marginally  
794 but significantly improve wetland area estimates. The estimates of global  
795 wetland potential/maximum is  $\sim 10.3$  Mkm<sup>2</sup>, with a mean annual maximum of  $\sim$   
796 5.17 Mkm<sup>2</sup> for 1980-2010. This development of the wetland modeling method  
797 reduces the uncertainties in modeling global wetland area and opens up new  
798 opportunities for studying the spatiotemporal variability of wetlands in LSMs  
799 that are directly comparable with inventories and satellite datasets.

800

### 801 **Acknowledgement**

802 Z. Zhang acknowledges funding by the CCES MAIOLICA2 project #42-01 and the  
803 National Natural Science Foundation of China (Y411391001). We are grateful to  
804 T. J. Bohn for providing WETCHIMP-WSL experiment results. We thank B. D.  
805 Stocker for providing HYDRO1K global river basin map. We thank T. Marthews  
806 for providing global CTI dataset of HydroSHEDS. We thank L. L. Hess for the  
807 results of dual-season inundated product of Lowland Amazon Basin.

808

809

### 810 **References**

811 | [Air Force Weather Agency: Data Format Handbook](#) for AGRMET, technical  
812 | report, Air Force Weather Agency's (AFWA) Agricultural Meteorological  
813 | modeling system (AGRMET), Air Force Weather Agency, [available at:](#)  
814 | [http://www2.mmm.ucar.edu/mm5/documents/DATA\\_FORMAT\\_HANDBOOK.pd](http://www2.mmm.ucar.edu/mm5/documents/DATA_FORMAT_HANDBOOK.pdf)  
815 | [f](#) (last access: July 2014), 2002.

816 | Bergamaschi, P., Frankenberg, C., Meirink, J. F., Krol, M., Dentener, F., Wagner, T.,  
817 | Platt, U., Kaplan, J. O., Körner, S., Heimann, M., Dlugokencky, E. J., and Goede, A.:  
818 | Satellite cartography of atmospheric methane from SCIAMACHY on board  
819 | ENVISAT: 2. Evaluation based on inverse model simulations, *Journal of*  
820 | *Geophysical Research: Atmospheres*, 112, D02304, 2007.

821 | Beven, K. J. and Cloke, H. L.: Comment on "Hyperresolution global land surface  
822 | modeling: Meeting a grand challenge for monitoring Earth's terrestrial water" by  
823 | Eric F. Wood et al, *Water Resources Research*, 48, W01801, 2012.

824 | Beven, K. J. and Kirkby, M. J.: A physically based, variable contributing area model  
825 | of basin hydrology / Un modèle à base physique de zone d'appel variable de  
826 | l'hydrologie du bassin versant, *Hydrological Sciences Bulletin*, 24, 43-69, 1979.

827 | Bindlish, R., Jackson, T. J., Gasiewski, A., Stankov, B., Klein, M., Cosh, M. H.,  
828 | Mladenova, I., Watts, C., Vivoni, E., Lakshmi, V., Bolten, J., and Keefer, T.: Aircraft  
829 | based soil moisture retrievals under mixed vegetation and topographic  
830 | conditions, *Remote Sensing of Environment*, 112, 375-390, 2008.

831 | [Bloom, A. A., Palmer, P. I., Fraser, A., and Reay, D. S.: Seasonal variability of](#)  
832 | [tropical wetland CH<sub>4</sub> emissions: the role of the methanogen-available carbon](#)  
833 | [pool, \*Biogeosciences\*, 9, 2821-2830, 2012.](#)

834 | [Bloom, A. A., Palmer, P. I., Fraser, A., Reay, D. S., and Frankenberg, C.: Large-Scale](#)  
835 | [Controls of Methanogenesis Inferred from Methane and Gravity Spaceborne](#)  
836 | [Data, \*Science\*, 327, 322-325, 2010.](#)

837 | Bohn, T. J., Melton, J. R., Ito, A., Kleinen, T., Spahni, R., Stocker, B. D., Zhang, B., Zhu,  
838 | X., Schroeder, R., Glagolev, M. V., Maksyutov, S., Brovkin, V., Chen, G., Denisov, S.  
839 | N., Eliseev, A. V., Gallego-Sala, A., McDonald, K. C., Rawlins, M. A., Riley, W. J.,  
840 | Subin, Z. M., Tian, H., Zhuang, Q., and Kaplan, J. O.: WETCHIMP-WSL:  
841 | intercomparison of wetland methane emissions models over West Siberia,  
842 | *Biogeosciences*, 12, 3321-3349, 2015.

843 | Bousquet, P., Ciais, P., Miller, J. B., Dlugokencky, E. J., Hauglustaine, D. A., Prigent,  
844 | C., Van der Werf, G. R., Peylin, P., Brunke, E. G., Carouge, C., Langenfelds, R. L.,  
845 | Lathiere, J., Papa, F., Ramonet, M., Schmidt, M., Steele, L. P., Tyler, S. C., and White,  
846 | J.: Contribution of anthropogenic and natural sources to atmospheric methane  
847 | variability, *Nature*, 443, 439-443, 2006.

848 | [Bousquet, P., Ringeval, B., Pison, I., Dlugokencky, E. J., Brunke, E. G., Carouge, C.,](#)  
849 | [Chevallier, F., Fortems-Cheiney, A., Frankenberg, C., Hauglustaine, D. A.,](#)  
850 | [Krummel, P. B., Langenfelds, R. L., Ramonet, M., Schmidt, M., Steele, L. P., Szopa,](#)  
851 | [S., Yver, C., Viovy, N., and Ciais, P.: Source attribution of the changes in](#)  
852 | [atmospheric methane for 2006–2008, \*Atmos. Chem. Phys.\*, 11, 3689-3700, 2011.](#)

853 | Brown, J., Ferrians, O. J., Jr., Heginbottom, J. A., and Melnikov, E. S.: Circum-arctic  
854 | map of permafrost and ground ice conditions, [edited by National Snow and Ice](#)  
855 | [Data Center, Boulder, CO, USA, available at:](#)  
856 | [http://nsidc.org/data/docs/fgdc/ggd318\\_map\\_circumarctic/](http://nsidc.org/data/docs/fgdc/ggd318_map_circumarctic/) (last access:  
857 | [December 2014](#)), 2001.

858 | Buytaert, W.: [TOPMODEL](http://cran.r-project.org/web/packages/topmodel/index.html), available at: [http://cran.r-](http://cran.r-project.org/web/packages/topmodel/index.html)  
859 | [project.org/web/packages/topmodel/index.html](http://cran.r-project.org/web/packages/topmodel/index.html), (last access: February 2015)  
860 | 2015.

861 | Chang, R. Y.-W., Miller, C. E., Dinardo, S. J., Karion, A., Sweeney, C., Daube, B. C.,  
862 | Henderson, J. M., Mountain, M. E., Eluszkiewicz, J., Miller, J. B., Bruhwiler, L. M. P.,  
863 | and Wofsy, S. C.: Methane emissions from Alaska in 2012 from CARVE airborne  
864 | observations, *Proceedings of the National Academy of Sciences*, doi:  
865 | 10.1073/pnas.1412953111, 2014. 2014.

866 | [Chen, X., Bohn, T. J., and Lettenmaier, D. P.: Model estimates of climate controls](#)  
867 | [on pan-Arctic wetland methane emissions, \*Biogeosciences\*, 12, 6259-6277, 2015.](#)  
868 | [Glagolev, M., Kleptsova, I., Filippov, I., Maksyutov, S., and Machida, T.: Regional](#)  
869 | [methane emission from West Siberia mire landscapes, \*Environmental Research\*](#)  
870 | [Letters, 6, 045214, 2011.](#)

871 | Collins, W. J., Bellouin, N., Doutriaux-Boucher, M., Gedney, N., Halloran, P., Hinton,  
872 | T., Hughes, J., Jones, C. D., Joshi, M., Liddicoat, S., Martin, G., O'Connor, F., Rae, J.,  
873 | Senior, C., Sitch, S., Totterdell, I., Wiltshire, A., and Woodward, S.: Development  
874 | and evaluation of an Earth-System model – HadGEM2, *Geosci. Model Dev.*, 4,  
875 | 1051-1075, 2011.

876 | Cosby, B. J., Hornberger, G. M., Clapp, R. B., and Ginn, T. R.: A Statistical  
877 | Exploration of the Relationships of Soil Moisture Characteristics to the Physical  
878 | Properties of Soils, *Water Resources Research*, 20, 682-690, 1984.

879 | Danielson, J. J. and Gesch, D. B.: Global Multi-resolution Terrain Elevation Data  
880 | 2010, available at [http://topotools.cr.usgs.gov/gmted\\_viewer/](http://topotools.cr.usgs.gov/gmted_viewer/) (last access:  
881 | [September 2014](#)), 2011.

882 | de Rosnay, P., Drusch, M., Vasiljevic, D., Balsamo, G., Albergel, C., and Isaksen, L.: A  
883 | simplified Extended Kalman Filter for the global operational soil moisture  
884 | analysis at ECMWF, *Quarterly Journal of the Royal Meteorological Society*, 139,  
885 | 1199-1213, 2013.

886 | Dorigo, W. A., Wagner, W., Hohensinn, R., Hahn, S., Paulik, C., Xaver, A., Gruber, A.,  
887 | Drusch, M., Mecklenburg, S., van Oevelen, P., Robock, A., and Jackson, T.: The  
888 | International Soil Moisture Network: a data hosting facility for global in situ soil  
889 | moisture measurements, *Hydrol. Earth Syst. Sci.*, 15, 1675-1698, 2011.

890 | Ducharne, A.: Reducing scale dependence in TOPMODEL using a dimensionless  
891 | topographic index, *Hydrol. Earth Syst. Sci.*, 13, 2399-2412, 2009.

892 | Durand, M., Lee-Lueng, F., Lettenmaier, D. P., Alsdorf, D. E., Rodriguez, E., and  
893 | Esteban-Fernandez, D.: The Surface Water and Ocean Topography Mission:  
894 | Observing Terrestrial Surface Water and Oceanic Submesoscale Eddies,  
895 | *Proceedings of the IEEE*, 98, 766-779, 2010.

896 | Entekhabi, D., Njoku, E. G., O'Neill, P. E., Kellogg, K. H., Crow, W. T., Edelstein, W.  
897 | N., Entin, J. K., Goodman, S. D., Jackson, T. J., Johnson, J., Kimball, J., Piepmeier, J. R.,  
898 | Koster, R. D., Martin, N., McDonald, K. C., Moghaddam, M., Moran, S., Reichle, R.,  
899 | Shi, J. C., Spencer, M. W., Thurman, S. W., Leung, T., and Van Zyl, J.: The Soil  
900 | Moisture Active Passive (SMAP) Mission, *Proceedings of the IEEE*, 98, 704-716,  
901 | 2010.

902 | Fan, Y., Li, H., and Miguez-Macho, G.: Global Patterns of Groundwater Table  
903 | Depth, *Science*, 339, 940-943, 2013.

904 | Fan, Y. and Miguez-Macho, G.: A simple hydrologic framework for simulating  
905 | wetlands in climate and earth system models, *Clim Dyn*, 37, 253-278, 2011.

906 Fisher, R. E., Sriskantharajah, S., Lowry, D., Lanoisellé, M., Fowler, C. M. R., James,  
907 R. H., Hermansen, O., Lund Myhre, C., Stohl, A., Greinert, J., Nisbet-Jones, P. B. R.,  
908 Mienert, J., and Nisbet, E. G.: Arctic methane sources: Isotopic evidence for  
909 atmospheric inputs, *Geophysical Research Letters*, 38, L21803, 2011.

910 Fluet-Chouinard, E., Lehner, B., Rebelo, L.-M., Papa, F., and Hamilton, S. K.:  
911 Development of a global inundation map at high spatial resolution from  
912 topographic downscaling of coarse-scale remote sensing data, *Remote Sensing of  
913 Environment*, 158, 348-361, 2015.

914 Gedney, N. and Cox, P. M.: The Sensitivity of Global Climate Model Simulations to  
915 the Representation of Soil Moisture Heterogeneity, *Journal of Hydrometeorology*,  
916 4, 1265-1275, 2003.

917 Gerten, D., Schaphoff, S., Haberlandt, U., Lucht, W., and Sitch, S.: Terrestrial  
918 vegetation and water balance—hydrological evaluation of a dynamic global  
919 vegetation model, *Journal of Hydrology*, 286, 249-270, 2004.

920 Glagolev, M., Kleptsova, I., Filippov, I., Maksyutov, S., and Machida, T.: Regional  
921 methane emission from West Siberia mire landscapes, *Environmental Research  
922 Letters*, 6, 045214, 2011.

923 Grabs, T., Seibert, J., Bishop, K., and Laudon, H.: Modeling spatial patterns of  
924 saturated areas: A comparison of the topographic wetness index and a dynamic  
925 distributed model, *Journal of Hydrology*, 373, 15-23, 2009.

926 [Gurney, K. R., Law, R. M., Denning, A. S., Rayner, P. J., Baker, D., Bousquet, P.,  
927 Bruhwiler, L., Chen, Y.-H., Ciais, P., Fan, S., Fung, I. Y., Gloor, M., Heimann, M.,  
928 Higuchi, K. A. Z., John, J., Kowalczyk, E. V. A., Maki, T., Maksyutov, S., Peylin, P.,  
929 Prather, M., Pak, B. C., Sarmiento, J., Taguchi, S., Takahashi, T., and Yuen, C.-W.:  
930 \[TransCom 3 CO<sub>2</sub> inversion intercomparison: 1. Annual mean control results and  
931 sensitivity to transport and prior flux information, \\*Tellus B\\*, 55, 555-579, 2003.\]\(#\)](#)

932 Güntner, A., Seibert, J., and Uhlenbrook, S.: Modeling spatial patterns of saturated  
933 areas: An evaluation of different terrain indices, *Water Resources Research*, 40,  
934 W05114, 2004.

935 Harris, I., Jones, P. D., Osborn, T. J., and Lister, D. H.: Updated high-resolution  
936 grids of monthly climatic observations – the CRU TS3.10 Dataset, *International  
937 Journal of Climatology*, 34, 623-642, 2014.

938 Hess, L., Melack, J., Affonso, A., Barbosa, C., Gastil-Buhl, M., and Novo, E. L. M.:  
939 Wetlands of the Lowland Amazon Basin: Extent, Vegetative Cover, and Dual-  
940 season Inundated Area as Mapped with JERS-1 Synthetic Aperture Radar,  
941 *Wetlands*, doi: 10.1007/s13157-015-0666-y, 2015. 1-12, 2015.

942 Hodson, E. L., Poulter, B., Zimmermann, N. E., Prigent, C., and Kaplan, J. O.: The El  
943 Niño–Southern Oscillation and wetland methane interannual variability,  
944 *Geophysical Research Letters*, 38, L08810, 2011.

945 IPCC: *Climate Change 2013: The Physical Science Basis. Contribution of Working  
946 Group I to the Fifth Assessment Report of the Intergovernmental Panel on  
947 Climate Change*, Cambridge University Press, Cambridge, United Kingdom and  
948 New York, NY, USA, 2013.

949 Ito, A. and Inatomi, M.: Use of a process-based model for assessing the methane  
950 budgets of global terrestrial ecosystems and evaluation of uncertainty,  
951 *Biogeosciences*, 9, 759-773, 2012.

952 Jennifer, D. W., John, S. K., Annett, B., and Kyle, C. M.: Surface water inundation in  
953 the boreal-Arctic: potential impacts on regional methane emissions,  
954 *Environmental Research Letters*, 9, 075001, 2014.

955 Junk, W., Piedade, M., Schöngart, J., Cohn-Haft, M., Adeney, J. M., and Wittmann, F.:  
956 A Classification of Major Naturally-Occurring Amazonian Lowland Wetlands,  
957 Wetlands, 31, 623-640, 2011.

958 Kaplan, J. O.: Wetlands at the Last Glacial Maximum: Distribution and methane  
959 emissions, Geophysical Research Letters, 29, 3-1-3-4, 2002.

960 Kerr, Y. H., Waldteufel, P., Wigneron, J. P., Delwart, S., Cabot, F., Boutin, J.,  
961 Escorihuela, M. J., Font, J., Reul, N., Gruhier, C., Juglea, S. E., Drinkwater, M. R.,  
962 Hahne, A., Martin-Neira, M., and Mecklenburg, S.: The SMOS Mission: New Tool  
963 for Monitoring Key Elements of the Global Water Cycle, Proceedings of the IEEE,  
964 98, 666-687, 2010.

965 Kim, Y., Kimball, J. S., Zhang, K., and McDonald, K. C.: Satellite detection of  
966 increasing Northern Hemisphere non-frozen seasons from 1979 to 2008:  
967 Implications for regional vegetation growth, Remote Sensing of Environment,  
968 121, 472-487, 2012.

969 Kirschke, S., Bousquet, P., Ciais, P., Saunois, M., Canadell, J. G., Dlugokencky, E. J.,  
970 Bergamaschi, P., Bergmann, D., Blake, D. R., Bruhwiler, L., Cameron-Smith, P.,  
971 Castaldi, S., Chevallier, F., Feng, L., Fraser, A., Heimann, M., Hodson, E. L.,  
972 Houweling, S., Josse, B., Fraser, P. J., Krummel, P. B., Lamarque, J.-F., Langenfelds,  
973 R. L., Le Quere, C., Naik, V., O'Doherty, S., Palmer, P. I., Pison, I., Plummer, D.,  
974 Poulter, B., Prinn, R. G., Rigby, M., Ringeval, B., Santini, M., Schmidt, M., Shindell,  
975 D. T., Simpson, I. J., Spahni, R., Steele, L. P., Strode, S. A., Sudo, K., Szopa, S., van der  
976 Werf, G. R., Voulgarakis, A., van Weele, M., Weiss, R. F., Williams, J. E., and Zeng,  
977 G.: Three decades of global methane sources and sinks, Nature Geosci, 6, 813-  
978 823, 2013.

979 Kleinen, T., Brovkin, V., and Schuldt, R. J.: A dynamic model of wetland extent and  
980 peat accumulation: results for the Holocene, Biogeosciences, 9, 235-248, 2012.

981 Kopecký, M. and Čížková, Š.: Using topographic wetness index in vegetation  
982 ecology: does the algorithm matter?, Applied Vegetation Science, 13, 450-459,  
983 2010.

984 [Kopecký, M. and Čížková, Š.: Using topographic wetness index in vegetation](#)  
985 [ecology: does the algorithm matter?, Applied Vegetation Science, 13, 450-459,](#)  
986 [2010.](#)

987 Leff, B., Ramankutty, N., and Foley, J. A.: Geographic distribution of major crops  
988 across the world, Global Biogeochemical Cycles, 18, GB1009, 2004.

989 Lehner, B. and Döll, P.: Development and validation of a global database of lakes,  
990 reservoirs and wetlands, Journal of Hydrology, 296, 1-22, 2004.

991 Lehner, B. and Grill, G.: Global river hydrography and network routing: baseline  
992 data and new approaches to study the world's large river systems, Hydrological  
993 Processes, 27, 2171-2186, 2013.

994 Lehner, B., Verdin, K., and Jarvis, A.: New Global Hydrography Derived From  
995 Spaceborne Elevation Data, Eos, Transactions American Geophysical Union, 89,  
996 93-94, 2008.

997 Lei, H., Huang, M., Leung, L. R., Yang, D., Shi, X., Mao, J., Hayes, D. J., Schwalm, C. R.,  
998 Wei, Y., and Liu, S.: Sensitivity of global terrestrial gross primary production to  
999 hydrologic states simulated by the Community Land Model using two runoff  
1000 parameterizations, Journal of Advances in Modeling Earth Systems, 6, 658-679,  
1001 2014.

1002 Liang, X., Lettenmaier, D. P., Wood, E. F., and Burges, S. J.: A simple hydrologically  
1003 based model of land surface water and energy fluxes for general circulation  
1004 models, *Journal of Geophysical Research: Atmospheres*, 99, 14415-14428, 1994.

1005 Lin, K., Zhang, Q., and Chen, X.: An evaluation of impacts of DEM resolution and  
1006 parameter correlation on TOPMODEL modeling uncertainty, *Journal of*  
1007 *Hydrology*, 394, 370-383, 2010.

1008 Lin, S., Jing, C., Coles, N., Chaplot, V., Moore, N., and Wu, J.: Evaluating DEM source  
1009 and resolution uncertainties in the Soil and Water Assessment Tool, *Stoch*  
1010 *Environ Res Risk Assess*, 27, 209-221, 2013.

1011 Marthews, T. R., Dadson, S. J., Lehner, B., Abele, S., and Gedney, N.: High-  
1012 resolution global topographic index values for use in large-scale hydrological  
1013 modelling, *Hydrol. Earth Syst. Sci.*, 19, 91-104, 2015.

1014 Marthews, T. R., Quesada, C. A., Galbraith, D. R., Malhi, Y., Mullins, C. E., Hodnett,  
1015 M. G., and Dharssi, I.: High-resolution hydraulic parameter maps for surface soils  
1016 in tropical South America, *Geosci. Model Dev.*, 7, 711-723, 2014.

1017 Matthews, E. and Fung, I.: Methane emission from natural wetlands: Global  
1018 distribution, area, and environmental characteristics of sources, *Global*  
1019 *Biogeochemical Cycles*, 1, 61-86, 1987.

1020 [Melack, J. M., Hess, L. L., Gastil, M., Forsberg, B. R., Hamilton, S. K., Lima, I. B. T.,](#)  
1021 [and Novo, E. M. L. M.: Regionalization of methane emissions in the Amazon Basin](#)  
1022 [with microwave remote sensing, \*Global Change Biology\*, 10, 530-544, 2004.](#)

1023 Melton, J. R., Wania, R., Hodson, E. L., Poulter, B., Ringeval, B., Spahni, R., Bohn, T.,  
1024 Avis, C. A., Beerling, D. J., Chen, G., Eliseev, A. V., Denisov, S. N., Hopcroft, P. O.,  
1025 Lettenmaier, D. P., Riley, W. J., Singarayer, J. S., Subin, Z. M., Tian, H., Zürcher, S.,  
1026 Brovkin, V., van Bodegom, P. M., Kleinen, T., Yu, Z. C., and Kaplan, J. O.: Present  
1027 state of global wetland extent and wetland methane modelling: conclusions from  
1028 a model inter-comparison project (WETCHIMP), *Biogeosciences*, 10, 753-788,  
1029 2013.

1030 Meng, L., Hess, P. G. M., Mahowald, N. M., Yavitt, J. B., Riley, W. J., Subin, Z. M.,  
1031 Lawrence, D. M., Swenson, S. C., Jauhiainen, J., and Fuka, D. R.: Sensitivity of  
1032 wetland methane emissions to model assumptions: application and model  
1033 testing against site observations, *Biogeosciences*, 9, 2793-2819, 2012.

1034 Mulligan, M. and Wainwright, J.: *Modelling and Model Building*, in:  
1035 *Environmental Modelling*, John Wiley & Sons, Ltd, [Chichester, UK, 7-26](#), 2013.

1036 Nachtergaele, F., Van Velthuizen, H., Verelst, L., Batjes, N., Dijkshoorn, K., Van  
1037 Engelen, V., Fischer, G., Jones, A., Montanarella, L., and Petri, M.: *Harmonized*  
1038 *world soil database*, FAO, Rome, Italy and IIASA, Laxenburg, Austria, 2008.

1039 Nisbet, E. G., Dlugokencky, E. J., and Bousquet, P.: Methane on the Rise—Again,  
1040 *Science*, 343, 493-495, 2014.

1041 [National Wetland Working Group: Wetlands of Canada. Ecological Land](#)  
1042 [Classification Series, No., 24. Canada Committee on Ecological Land](#)  
1043 [Classification, Sustainable Development Branch, Environment Canada and](#)  
1044 [Polyscience Publications Inc, Montreal, Quebec, Canada.](#)

1045 Niu, G.-Y., Yang, Z.-L., Dickinson, R. E., and Gulden, L. E.: A simple TOPMODEL-  
1046 based runoff parameterization (SIMTOP) for use in global climate models,  
1047 *Journal of Geophysical Research: Atmospheres*, 110, D21106, 2005.

1048 Pan, F., Peters-Lidard, C. D., Sale, M. J., and King, A. W.: A comparison of  
1049 geographical information systems-based algorithms for computing the  
1050 TOPMODEL topographic index, *Water Resources Research*, 40, W06303, 2004.

1051 Papa, F., Prigent, C., Aires, F., Jimenez, C., Rossow, W. B., and Matthews, E.:  
1052 Interannual variability of surface water extent at the global scale, 1993–2004,  
1053 Journal of Geophysical Research: Atmospheres, 115, D12111, 2010.

1054 Peregon, A., Maksyutov, S., Kosykh, N. P., and Mironycheva-Tokareva, N. P.: Map-  
1055 based inventory of wetland biomass and net primary production in western  
1056 Siberia, Journal of Geophysical Research: Biogeosciences, 113, G01007, 2008.

1057 Petrescu, A. M. R., Lohila, A., Tuovinen, J.-P., Baldocchi, D. D., Desai, A. R., Roulet,  
1058 N. T., Vesala, T., Dolman, A. J., Oechel, W. C., Marcolla, B., Friborg, T., Rinne, J.,  
1059 Matthes, J. H., Merbold, L., Meijide, A., Kiely, G., Sottocornola, M., Sachs, T., Zona,  
1060 D., Varlagin, A., Lai, D. Y. F., Veenendaal, E., Parmentier, F.-J. W., Skiba, U., Lund,  
1061 M., Hensen, A., van Huissteden, J., Flanagan, L. B., Shurpali, N. J., Grünwald, T.,  
1062 Humphreys, E. R., Jackowicz-Korczyński, M., Aurela, M. A., Laurila, T., Grüning, C.,  
1063 Corradi, C. A. R., Schrier-Uijl, A. P., Christensen, T. R., Tamstorf, M. P., Mastepanov,  
1064 M., Martikainen, P. J., Verma, S. B., Bernhofer, C., and Cescatti, A.: The uncertain  
1065 climate footprint of wetlands under human pressure, Proceedings of the National  
1066 Academy of Sciences, 112, 4594-4599, 2015.

1067 Petrescu, A. M. R., van Beek, L. P. H., van Huissteden, J., Prigent, C., Sachs, T.,  
1068 Corradi, C. A. R., Parmentier, F. J. W., and Dolman, A. J.: Modeling regional to  
1069 global CH<sub>4</sub> emissions of boreal and arctic wetlands, Global Biogeochemical  
1070 Cycles, 24, GB4009, 2010.

1071 Poulter, B., Ciais, P., Hodson, E., Lischke, H., Maignan, F., Plummer, S., and  
1072 Zimmermann, N. E.: Plant functional type mapping for earth system models,  
1073 Geosci. Model Dev., 4, 993-1010, 2011.

1074 [Poulter, B., Bousquet, P., Canadell, P., Ciais, P., Peregon, A., Arora, V., Beerling, D.,](#)  
1075 [Brovkin, V., Hopcroft, P., Jones, C., Joos, F., Gedney, N., Ito, A., Kleinen, T., Koven,](#)  
1076 [C., MacDonald, K., Melton, J., Peng, C., Peng, S., Schroder, R., Prigent, C., Riley, B.,](#)  
1077 [Saito, M., Spahni, R., Tian, H., Taylor, L., Viovy, N., Wilton, D., Wiltshire, A., Xu, X.,](#)  
1078 [and Zhang, Z.: Global wetland contribution to increasing atmospheric methane](#)  
1079 [concentrations \(2000-2012\), in preparation, 2015.](#)

1080 Prigent, C., Papa, F., Aires, F., Jimenez, C., Rossow, W. B., and Matthews, E.:  
1081 Changes in land surface water dynamics since the 1990s and relation to  
1082 population pressure, Geophysical Research Letters, 39, L08403, 2012.

1083 Prigent, C., Papa, F., Aires, F., Rossow, W. B., and Matthews, E.: Global inundation  
1084 dynamics inferred from multiple satellite observations, 1993–2000, Journal of  
1085 Geophysical Research: Atmospheres, 112, D12107, 2007.

1086 Quinn, P. F., Beven, K. J., and Lamb, R.: The in(a/tan/β) index: How to calculate it  
1087 and how to use it within the topmodel framework, Hydrological Processes, 9,  
1088 161-182, 1995.

1089 Quiquet, A., Archibald, A. T., Friend, A. D., Chappellaz, J., Levine, J. G., Stone, E. J.,  
1090 Telford, P. J., and Pyle, J. A.: The relative importance of methane sources and  
1091 sinks over the Last Interglacial period and into the last glaciation, Quaternary  
1092 Science Reviews, 112, 1-16, 2015.

1093 Ringeval, B., Decharme, B., Piao, S. L., Ciais, P., Papa, F., de Noblet-Ducoudré, N.,  
1094 Prigent, C., Friedlingstein, P., Gouttevin, I., Koven, C., and Ducharne, A.: Modelling  
1095 sub-grid wetland in the ORCHIDEE global land surface model: evaluation against  
1096 river discharges and remotely sensed data, Geosci. Model Dev., 5, 941-962, 2012.

1097 Ringeval, B., Houweling, S., van Bodegom, P. M., Spahni, R., van Beek, R., Joos, F.,  
1098 and Röckmann, T.: Methane emissions from floodplains in the Amazon Basin:

1099 challenges in developing a process-based model for global applications,  
 1100 *Biogeosciences*, 11, 1519-1558, 2014.  
 1101 Rinne, J., Riutta, T., Pihlatie, M., Aurela, M., Haapanala, S., Tuovinen, J.-P., Tuittila,  
 1102 E.-S., and Vesala, T.: Annual cycle of methane emission from a boreal fen  
 1103 measured by the eddy covariance technique, *Tellus B*, 59, 449-457, 2007.  
 1104 Seneviratne, S. I., Corti, T., Davin, E. L., Hirschi, M., Jaeger, E. B., Lehner, I.,  
 1105 Orłowsky, B., and Teuling, A. J.: Investigating soil moisture–climate interactions  
 1106 in a changing climate: A review, *Earth-Science Reviews*, 99, 125-161, 2010.  
 1107 Sheng, Y., Smith, L. C., MacDonald, G. M., Kremenetski, K. V., Frey, K. E., Velichko,  
 1108 A. A., Lee, M., Beilman, D. W., and Dubinin, P.: A high-resolution GIS-based  
 1109 inventory of the west Siberian peat carbon pool, *Global Biogeochemical Cycles*,  
 1110 18, GB3004, 2004.  
 1111 Singarayer, J. S., Valdes, P. J., Friedlingstein, P., Nelson, S., and Beerling, D. J.: Late  
 1112 Holocene methane rise caused by orbitally controlled increase in tropical  
 1113 sources, *Nature*, 470, 82-85, 2011.  
 1114 Sitch, S., Smith, B., Prentice, I. C., Arneth, A., Bondeau, A., Cramer, W., Kaplan, J. O.,  
 1115 Levis, S., Lucht, W., Sykes, M. T., Thonicke, K., and Venevsky, S.: Evaluation of  
 1116 ecosystem dynamics, plant geography and terrestrial carbon cycling in the LPJ  
 1117 dynamic global vegetation model, *Global Change Biology*, 9, 161-185, 2003.  
 1118 Sivapalan, M., Beven, K., and Wood, E. F.: On hydrologic similarity: 2. A scaled  
 1119 model of storm runoff production, *Water Resources Research*, 23, 2266-2278,  
 1120 1987.  
 1121 Sørensen, R. and Seibert, J.: Effects of DEM resolution on the calculation of  
 1122 topographical indices: TWI and its components, *Journal of Hydrology*, 347, 79-  
 1123 89, 2007.  
 1124 Spahni, R., Wania, R., Neef, L., van Weele, M., Pison, I., Bousquet, P., Frankenberg,  
 1125 C., Foster, P. N., Joos, F., Prentice, I. C., and van Velthoven, P.: Constraining global  
 1126 methane emissions and uptake by ecosystems, *Biogeosciences*, 8, 1643-1665,  
 1127 2011.  
 1128 Stieglitz, M., Rind, D., Famiglietti, J., and Rosenzweig, C.: An Efficient Approach to  
 1129 Modeling the Topographic Control of Surface Hydrology for Regional and Global  
 1130 Climate Modeling, *Journal of Climate*, 10, 118-137, 1997.  
 1131 Stocker, B. D., Roth, R., Joos, F., Spahni, R., Steinacher, M., Zaehle, S., Bouwman, L.,  
 1132 Xu, R., and Prentice, I. C.: Multiple greenhouse-gas feedbacks from the land  
 1133 biosphere under future climate change scenarios, *Nature Clim. Change*, 3, 666-  
 1134 672, 2013.  
 1135 Stocker, B. D., Spahni, R., and Joos, F.: DYPTOP: a cost-efficient TOPMODEL  
 1136 implementation to simulate sub-grid spatio-temporal dynamics of global  
 1137 wetlands and peatlands, *Geosci. Model Dev.*, 7, 3089-3110, 2014.  
 1138 Tarnocai, C., Canadell, J. G., Schuur, E. A. G., Kuhry, P., Mazhitova, G., and Zimov, S.:  
 1139 Soil organic carbon pools in the northern circumpolar permafrost region, *Global*  
 1140 *Biogeochemical Cycles*, 23, GB2023, 2009.  
 1141 Turetsky, M. R., Kotowska, A., Bubier, J., Dise, N. B., Crill, P., Hornibrook, E. R. C.,  
 1142 Minkinen, K., Moore, T. R., Myers-Smith, I. H., Nykänen, H., Olefeldt, D., Rinne, J.,  
 1143 Saarnio, S., Shurpali, N., Tuittila, E.-S., Waddington, J. M., White, J. R., Wickland, K.  
 1144 P., and Wilmking, M.: A synthesis of methane emissions from 71 northern,  
 1145 temperate, and subtropical wetlands, *Global Change Biology*, 20, 2183-2197,  
 1146 | 2014.

1147 | [USGS: HYDRO1k Elevation Derivative Database, US Geological Survey Earth](#)  
1148 | [Resources Observation and Science \(EROS\) Data Center \(EDC\), Sioux Falls, South](#)  
1149 | [Dakota, USA, 1996.](#)

1150 | Verpoorter, C., Kutser, T., Seekell, D. A., and Tranvik, L. J.: A global inventory of  
1151 | lakes based on high-resolution satellite imagery, *Geophysical Research Letters*,  
1152 | 41, 6396-6402, 2014.

1153 | Wania, R., Melton, J. R., Hodson, E. L., Poulter, B., Ringeval, B., Spahni, R., Bohn, T.,  
1154 | Avis, C. A., Chen, G., Eliseev, A. V., Hopcroft, P. O., Riley, W. J., Subin, Z. M., Tian, H.,  
1155 | van Bodegom, P. M., Kleinen, T., Yu, Z. C., Singarayer, J. S., Zürcher, S.,  
1156 | Lettenmaier, D. P., Beerling, D. J., Denisov, S. N., Prigent, C., Papa, F., and Kaplan, J.  
1157 | O.: Present state of global wetland extent and wetland methane modelling:  
1158 | methodology of a model inter-comparison project (WETCHIMP), *Geosci. Model*  
1159 | *Dev.*, 6, 617-641, 2013.

1160 | Wania, R., Ross, I., and Prentice, I. C.: Integrating peatlands and permafrost into a  
1161 | dynamic global vegetation model: 1. Evaluation and sensitivity of physical land  
1162 | surface processes, *Global Biogeochemical Cycles*, 23, GB3014, 2009.

1163 | Ward, R. C. and Robinson, M.: Principles of [Hydrology](#), 4th Edn, McGraw-Hill,  
1164 | Maidenhead, UK, 2000.

1165 | Whalen, S. C. and Reeburgh, W. S.: Interannual variations in tundra methane  
1166 | emission: A 4-year time series at fixed sites, *Global Biogeochemical Cycles*, 6,  
1167 | 139-159, 1992.

1168 | Wilson, J. P. and Gallant, J. C.: *Terrain analysis: principles and applications*, John  
1169 | Wiley & Sons, New York, NY, [USA](#), 2000.

1170 | Wood, E. F., Roundy, J. K., Troy, T. J., van Beek, L. P. H., Bierkens, M. F. P., Blyth, E.,  
1171 | de Roo, A., Döll, P., Ek, M., Famiglietti, J., Gochis, D., van de Giesen, N., Houser, P.,  
1172 | Jaffé, P. R., Kollet, S., Lehner, B., Lettenmaier, D. P., Peters-Lidard, C., Sivapalan, M.,  
1173 | Sheffield, J., Wade, A., and Whitehead, P.: Hyperresolution global land surface  
1174 | modeling: Meeting a grand challenge for monitoring Earth's terrestrial water,  
1175 | *Water Resources Research*, 47, W05301, 2011.

1176 | Woodward, C., Shulmeister, J., Larsen, J., Jacobsen, G. E., and Zawadzki, A.: The  
1177 | hydrological legacy of deforestation on global wetlands, *Science*, 346, 844-847,  
1178 | 2014.

1179 | [Zhang, Z., Jiang, H., Liu, J., Ju, W., and Zhang, X.: Effect of heterogeneous](#)  
1180 | [atmospheric CO<sub>2</sub> on simulated global carbon budget, \*Global and Planetary\*](#)  
1181 | [Change, 101, 33-51, 2013.](#)

1182 | Zhu, X., Zhuang, Q., Lu, X., and Song, L.: Spatial scale-dependent land-atmospheric  
1183 | methane exchanges in the northern high latitudes from 1993 to 2004,  
1184 | *Biogeosciences*, 11, 1693-1704, 2014.

1185 | [Zhuang, Q., Melillo, J. M., Kicklighter, D. W., Prinn, R. G., McGuire, A. D., Steudler, P.](#)  
1186 | [A., Felzer, B. S., and Hu, S.: Methane fluxes between terrestrial ecosystems and](#)  
1187 | [the atmosphere at northern high latitudes during the past century: A](#)  
1188 | [retrospective analysis with a process-based biogeochemistry model, \*Global\*](#)  
1189 | [Biogeochemical Cycles](#), 18, GB3010, 2004.

1190 | Zona, D., Oechel, W. C., Kochendorfer, J., Paw U, K. T., Salyuk, A. N., Olivas, P. C.,  
1191 | Oberbauer, S. F., and Lipson, D. A.: Methane fluxes during the initiation of a large-  
1192 | scale water table manipulation experiment in the Alaskan Arctic tundra, *Global*  
1193 | *Biogeochemical Cycles*, 23, GB2013, 2009.

1194 Zürcher, S., Spahni, R., Joos, F., Steinacher, M., and Fischer, H.: Impact of an abrupt  
1195 cooling event on interglacial methane emissions in northern peatlands,  
1196 | Biogeosciences, 10, 1963-1981, 2013.

## Tables

Table 1. Soil parameters for LPJ-wsl soil classes.  $f$  is a parameter describing the exponential decline of transmissivity with depth for each soil type.

Soil type	$f$	Mineral Content (%)	Organic Content (%)	Wilting Point (%)	Porosity (%)
Clay Heavy	3.2	0.508	0.01	0.138	0.138
Silty Clay	3.1	0.531	0.01	0.126	0.468
Clay	2.8	0.531	0.01	0.138	0.468
Silty Clay Loam	2.9	0.534	0.01	0.120	0.464
Clay Loam	2.7	0.595	0.01	0.103	0.465
Silt	3.4	0.593	0.01	0.084	0.476
Silt Loam	2.6	0.593	0.01	0.084	0.476
Sandy Clay	2.5	0.535	0.01	0.100	0.406
Loam	2.5	0.535	0.01	0.066	0.439
Sandy Clay Loam	2.4	0.565	0.01	0.067	0.404
Sandy Loam	2.3	0.565	0.01	0.047	0.434
Loamy Sand	2.2	0.578	0.01	0.028	0.421
Sand	2.1	0.578	0.01	0.010	0.339
Organic	2.5	0.01	0.20	0.066	0.439

Table 2 Model experiments for different parameterization schemes and corresponding DEM products applied in this study.

Model Experiment	DEM	DEM source	Resolution (arc seconds)	Coverage	River Basin	Aggregation type	Hydro-corrected
HYDRO1k_BASIN	Hydro1k	GTOPO30	30	Global*	HYDRO1K	Catchment	Yes
HYDRO1k_GRID	Hydro1k	GTOPO30	30	Global*	HYDRO1K	Grid	Yes
GMTED_BASIN	GMTED	SRTM&others	15	Global	HYDRO1K	Catchment	No
GMTED_GRID	GMTED	SRTM&others	15	Global	HYDRO1K	Grid	No
SHEDS_BASIN	HydroSHEDS	SRTM	15	<60°N	HydroSHEDS	Catchment	Yes
SHEDS_GRID	HydroSHEDS	SRTM	15	<60°N	HydroSHEDS	Grid	Yes

Table 3 Summary of simulated and observed mean annual minimum (MIN), maximum (MAX), and amplitude (AMP) of wetland extent for 1980-2010. All units are Mkm<sup>2</sup> (106 km<sup>2</sup>) ± 1σ, where standard deviation represents the inter-annual variation in model estimates except for the row Average, which represents uncertainties of estimates from each model experiment.

Model	Lowland Amazon Basin			West Siberian Lowland			Global		
	MIN	MAX	AMP	MIN	MAX	AMP	MIN	MAX	AMP
SHEDS_BASIN	0.27±0.02	0.38±0.01	0.11±0.01	0±0	0.45±0.05	0.45±0.05	2.96±0.06	5.17±0.11	2.23±0.10
SHEDS_GRID	0.32±0.01	0.40±0.01	0.08±0.01	0±0	0.45±0.05	0.45±0.05	3.56±0.06	5.93±0.11	2.38±0.10
GMTED_BASIN	0.21±0.02	0.35±0.01	0.14±0.02	0±0	0.39±0.06	0.39±0.06	2.09±0.05	3.75±0.12	1.66±0.12
GMTED_GRID	0.19±0.02	0.34±0.01	0.15±0.02	0±0	0.38±0.06	0.38±0.06	1.80±0.05	3.32±0.13	1.52±0.13
HYDRO1k_BASIN	0.25±0.02	0.37±0.01	0.12±0.01	0±0	0.39±0.06	0.39±0.06	2.44±0.05	4.32±0.11	1.89±0.11
HYDRO1k_GRID	0.22±0.02	0.36±0.01	0.14±0.02	0±0	0.36±0.07	0.36±0.07	2.12±0.05	3.73±0.13	1.61±0.13
<b>Average</b>	<b>0.27±0.04</b>	<b>0.38±0.02</b>	<b>0.11±0.01</b>	<b>0±0</b>	<b>0.40±0.04</b>	<b>0.40±0.04</b>	<b>2.49±0.65</b>	<b>4.37±0.99</b>	<b>1.88±0.35</b>
Observations									
Hess2015	0.23	0.58							
GIEMS	0.12±0.01	0.25±0.03	0.14±0.04	0±0	0.24±0.05	0.25±0.05	1.38±0.09	4.47±0.20	3.09±0.19
SWAMPS-GLWD	0.22±0.03	0.34±0.01	0.12±0.03	0±0	0.50±0.03	0.51±0.03	3.03±0.13	6.62±0.18	3.63±0.14

Table 4 Spearman correlations between satellite-based vs. modeled interannual anomalies of the grid-cells contained in each region defined in Fig. 2f at global scale. Values out and in parentheses are correlation efficient with SWAMPS-GLWD and GIEMS respectively. The two highest value within one column is in bold.

Regions	SHDES BASIN	SHDES GRID	GMTED BASIN	GMTED GRID	HYDRO1K BASIN	HYDRO1k GRID
Boreal North America	<b>0.770</b> ( <b>0.378</b> )	<b>0.768</b> (0.376)	0.751 (0.354)	0.745 (0.341)	0.765 ( <b>0.378</b> )	0.748 (0.343)
Boreal Eurasia	<b>0.785</b> ( <b>0.513</b> )	<b>0.782</b> ( <b>0.511</b> )	0.763 (0.487)	0.764 (0.487)	0.763 (0.493)	0.760 (0.484)
Europe	<b>0.604</b> (0.091)	<b>0.595</b> (0.079)	0.313 (-0.198)	0.211 ( <b>-0.278</b> )	0.588 (0.076)	0.218 ( <b>-0.272</b> )
Tropical South America	0.723 ( <b>0.838</b> )	<b>0.725</b> (0.831)	0.724 (0.835)	0.666 (0.825)	0.708 ( <b>0.836</b> )	<b>0.726</b> (0.835)
South Africa	0.082 ( <b>0.736</b> )	0.044 (0.725)	<b>0.084</b> (0.735)	0.076 (0.734)	0.040 (0.717)	<b>0.088</b> ( <b>0.740</b> )
Tropical Asia	<b>0.689</b> ( <b>0.674</b> )	<b>0.681</b> (0.673)	0.705 ( <b>0.682</b> )	0.677 (0.625)	0.670 (0.660)	0.648 (0.632)
Temperate North America	0.359 (0.139)	0.380 (0.155)	0.406 (0.262)	0.347 (0.229)	<b>0.518</b> ( <b>0.288</b> )	<b>0.479</b> ( <b>0.305</b> )
Temperate South America	<b>-0.193</b> ( <b>0.633</b> )	<b>-0.205</b> (0.597)	-0.153 (0.622)	-0.162 ( <b>0.641</b> )	-0.178 (0.627)	-0.166 (0.627)
Temperate Eurasia	<b>0.742</b> ( <b>0.645</b> )	<b>0.760</b> ( <b>0.660</b> )	0.735 (0.642)	0.721 (0.643)	0.732 (0.642)	0.716 (0.642)

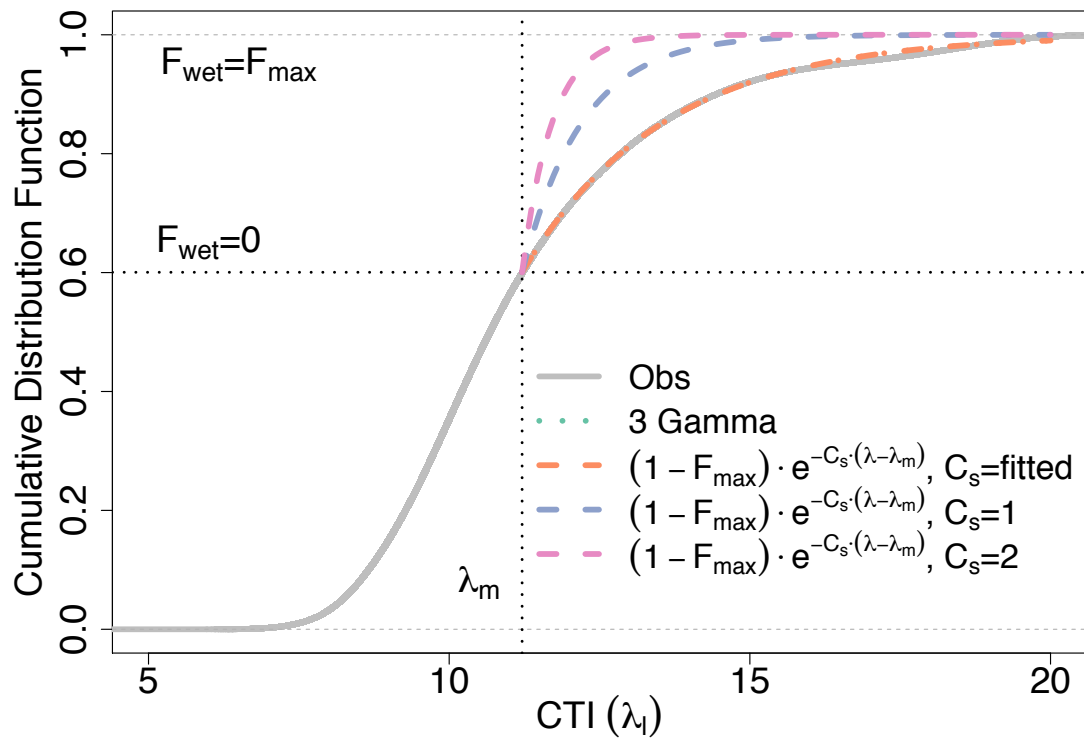
Table 5. List of global and regional wetland CH<sub>4</sub> estimates from our model experiments (see Table 2) over the period 1980-2000. All units are Tg CH<sub>4</sub> yr<sup>-1</sup>±1σ, where standard deviation represents the interannual variation in the model estimates. Note that estimates from some reference studies are not for the same period.

Estimates	Global	Regions			Hotspot			
		Tropics (20N-30S)	Temperate (20-45N, 30S-50S)	Northern (>45N)	Central Amazon <sup>b</sup>	WSL	Hudson Bay	Alaska
<u>SHEDS BASIN</u>	<u>171.9</u>	<u>109.3±2.3</u>	<u>26.4±1.0</u>	<u>36.1±1.8</u>	<u>10.9±0.3</u>	<u>5.4±0.9</u>	<u>6.5±0.5</u>	<u>1.7±0.3</u>
<u>SHEDS GRID</u>	<u>193.0</u>	<u>123.7±2.2</u>	<u>31.4±1.0</u>	<u>38.7±1.9</u>	<u>11.4±0.3</u>	<u>5.5±0.9</u>	<u>7.1±0.6</u>	<u>1.5±0.3</u>
<u>GMTED BASIN</u>	<u>130.1</u>	<u>85.5±2.3</u>	<u>19.0±0.9</u>	<u>26.3±1.4</u>	<u>9.5±0.4</u>	<u>4.5±0.9</u>	<u>4.4±0.6</u>	<u>1.6±0.3</u>
<u>GMTED GRID</u>	<u>117.2</u>	<u>76.7±2.3</u>	<u>16.4±0.9</u>	<u>24.2±1.4</u>	<u>9.2±0.4</u>	<u>4.1±0.9</u>	<u>4.2±0.6</u>	<u>1.4±0.3</u>
<u>HYDRO1K BASIN</u>	<u>148.3</u>	<u>96.4±2.3</u>	<u>21.5±0.9</u>	<u>30.3±1.6</u>	<u>10.4±0.3</u>	<u>4.4±0.9</u>	<u>5.8±0.6</u>	<u>1.7±0.3</u>
<u>HYDRO1K GRID</u>	<u>128.8</u>	<u>85.0±2.3</u>	<u>17.8±0.9</u>	<u>26.0±1.4</u>	<u>10.0±0.4</u>	<u>3.9±0.9</u>	<u>4.8±0.6</u>	<u>1.5±0.3</u>
Melton et al. (2013) <sup>a</sup>	<u>190±39</u>						<u>5.4±3.2</u>	
Zhu et al. (2015)	<u>209-245</u>			<u>38.1-55.4</u>				
Chen et al. (2015)				<u>35</u>			<u>3.11±0.45</u>	
Zhu et al. (2014)				<u>34-58</u>			<u>3.1±0.5</u>	
Ringeval et al. (2012)	<u>193.8</u>	<u>102</u>	<u>51</u>	<u>40.8</u>				
Glagolev et al. (2011)						<u>3.91±1.3</u>		
Melack et al. (2004)					<u>9.1</u>			
Zhuang et al. (2004)				<u>57.3</u>				
Chang et al. (2014)								<u>2.1±0.5</u>
Bloom et al. (2012)		<u>111.1</u>						
Bousquet et al. (2011)	<u>151±10</u>	<u>91±11</u>						
Bloom et al. (2010)	<u>165±50</u>	<u>91±28</u>					<u>4.9±1.4</u>	

<sup>a</sup> WETCHIMP estimates for 1993-2004

<sup>b</sup> Central Amazon (54-72°W,0-8°S)

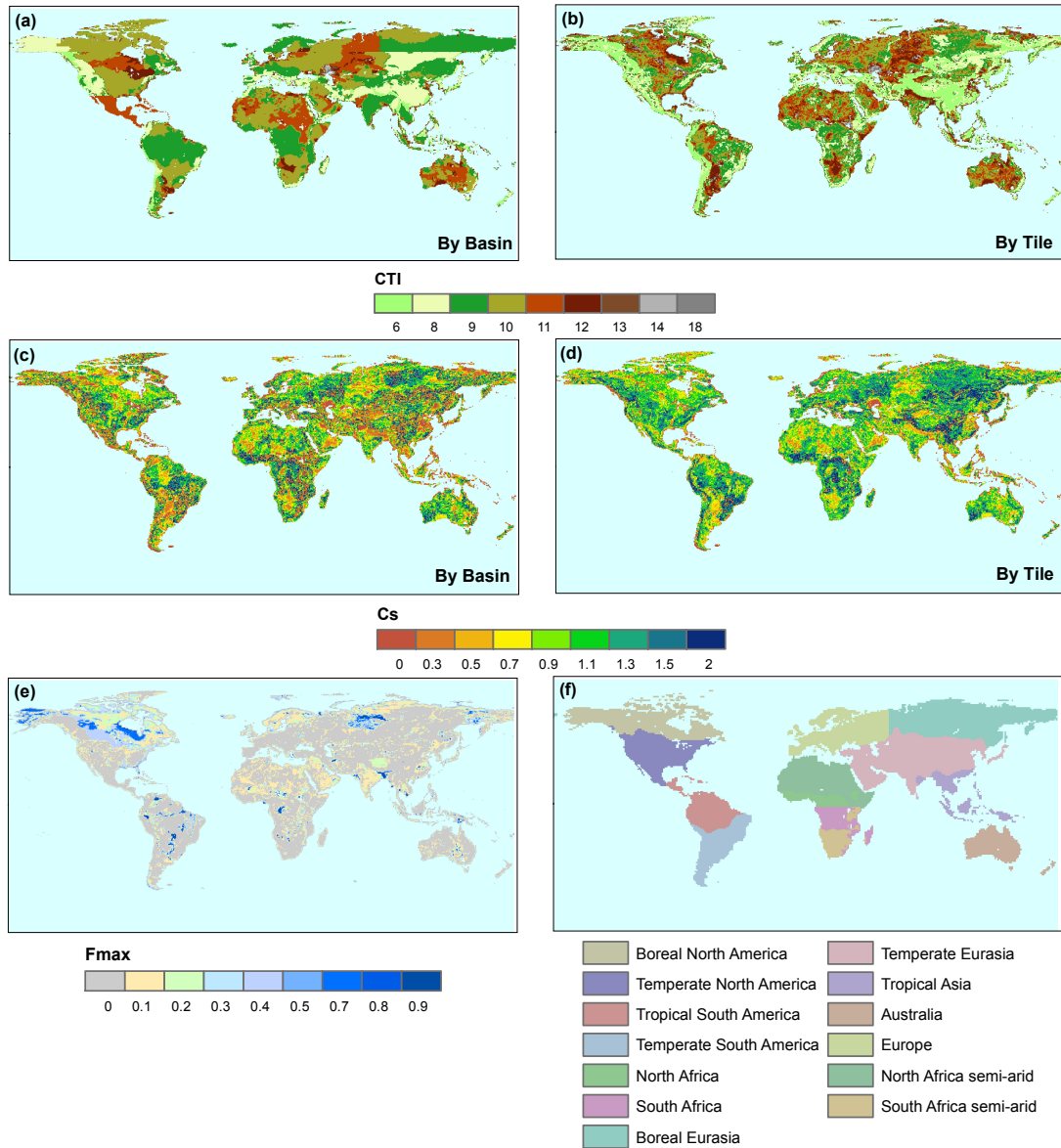
1 **Figures**



2

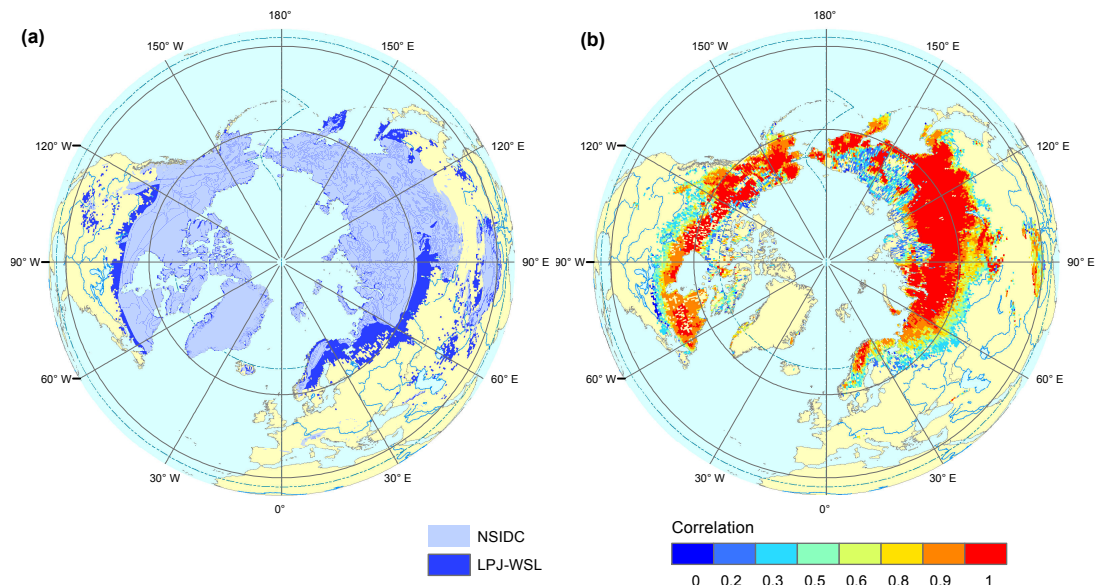
3 Figure 1. Cumulative distribution function (CDF) of the fitted exponential curve  
 4 (blue line) as a function of compound topographic index (CTI) in comparison  
 5 with the three-parameter gamma function (red line), as well as the observations  
 6 (grey line) with in a sample grid box.

7



8

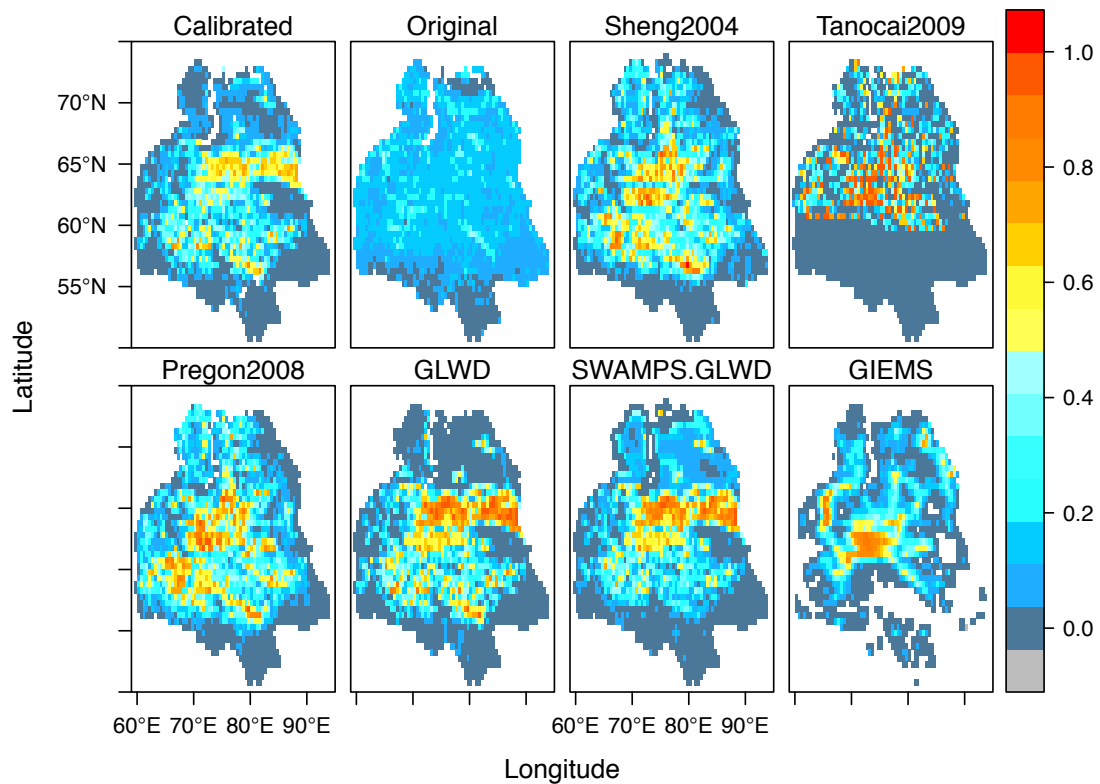
9 Figure 2. TOPMODEL parameter maps in model experiments. Mean CTI (a, b) and  
 10  $C_s$  (c, d) aggregated by river basin (denoted as “By Basin”) and grid cell (denoted  
 11 as “By Tile”) schemes from HydroSHEDS were listed.  $F_{max}$  (e) for calibration was  
 12 generated using SWAMPS-GLWD and GLWD. Map of regions (f) was used to  
 13 partition globe into boreal, temperate, tropical biomes (Gurney et al. 2003).  
 14



15

16 Figure 3 Evaluation of permafrost simulation in LPJ-wsl. (a) Inventory-based  
 17 (light blue) and simulated (dark blue) permafrost extent from NSIDC and LPJ-wsl  
 18 respectively. The inventory contains discontinuous, sporadic or isolated  
 19 permafrost boundaries, as well as the location of subsea and relict permafrost.  
 20 We only compare the distribution of all permafrost against model outputs  
 21 without distinguishing each permafrost types. (b) Spatial distribution of  
 22 Spearman correlation between simulated monthly frozen-days from LPJ-wsl  
 23 over 2002-2011 and satellite retrievals of FT status from AMSR-E.

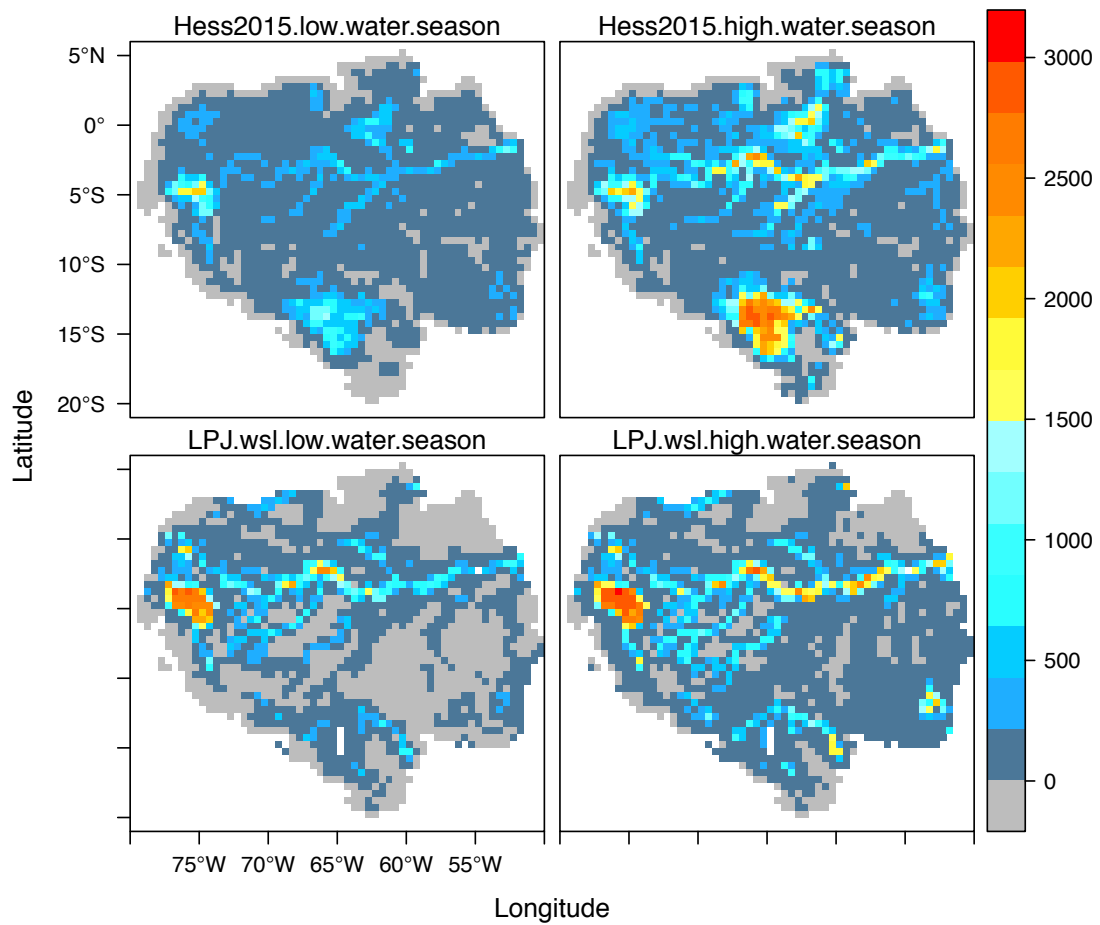
24



25

26 Figure 4 Comparison of TOPMODEL-based wetland areas and Observational  
 27 datasets over the region West Siberian Lowland (WSL) for June-July-August (JJA)  
 28 average over the period 1993-2012. 'Calibrated' and 'Original' represent  
 29 simulated wetland areas with and without  $F_{max}$  calibration respectively. For  
 30 Sheng2004, Tanocai, Pregon2008, and GLWD, it represents maximum wetland  
 31 extent per  $0.5^\circ$  cell as derived from static inventory maps. For SWAMPS-GLWD  
 32 and GIEMS, areas shown are averaged for JJA over the period 1993-2007 and  
 33 2000-2012 respectively.

34

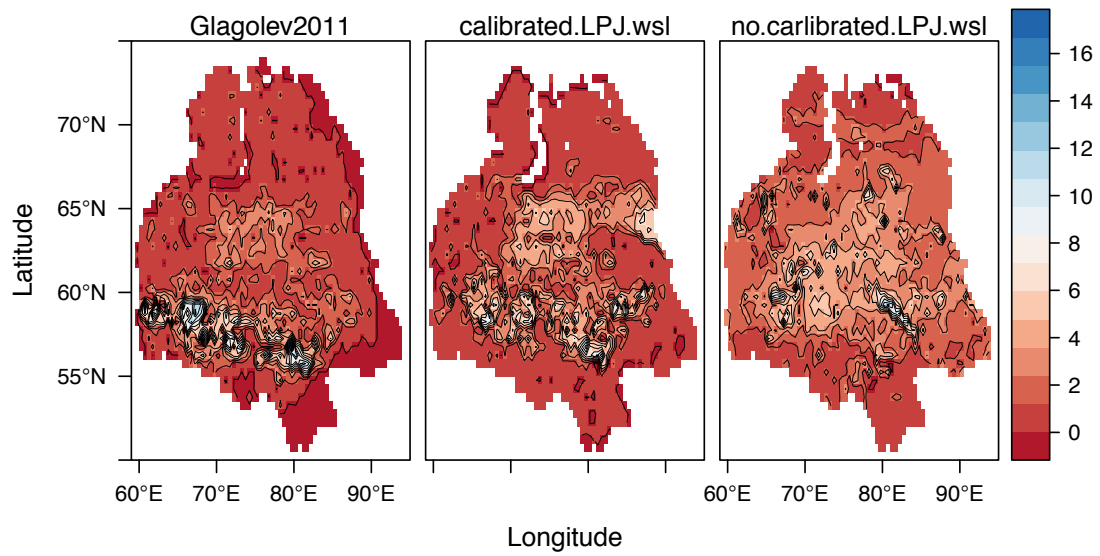


35

36 Figure 5. Comparison of wetland areas (km<sup>2</sup>) between LPJ-wsl simulated results  
 37 (SHEDS\_basin version) and JERS-1 satellite observation over Lowland Amazon  
 38 Basin for low-water season and high-water season. The low water season and  
 39 high-water season in LPJ was calculated by mean annual minimum and  
 40 maximum respectively during 1993-2013.

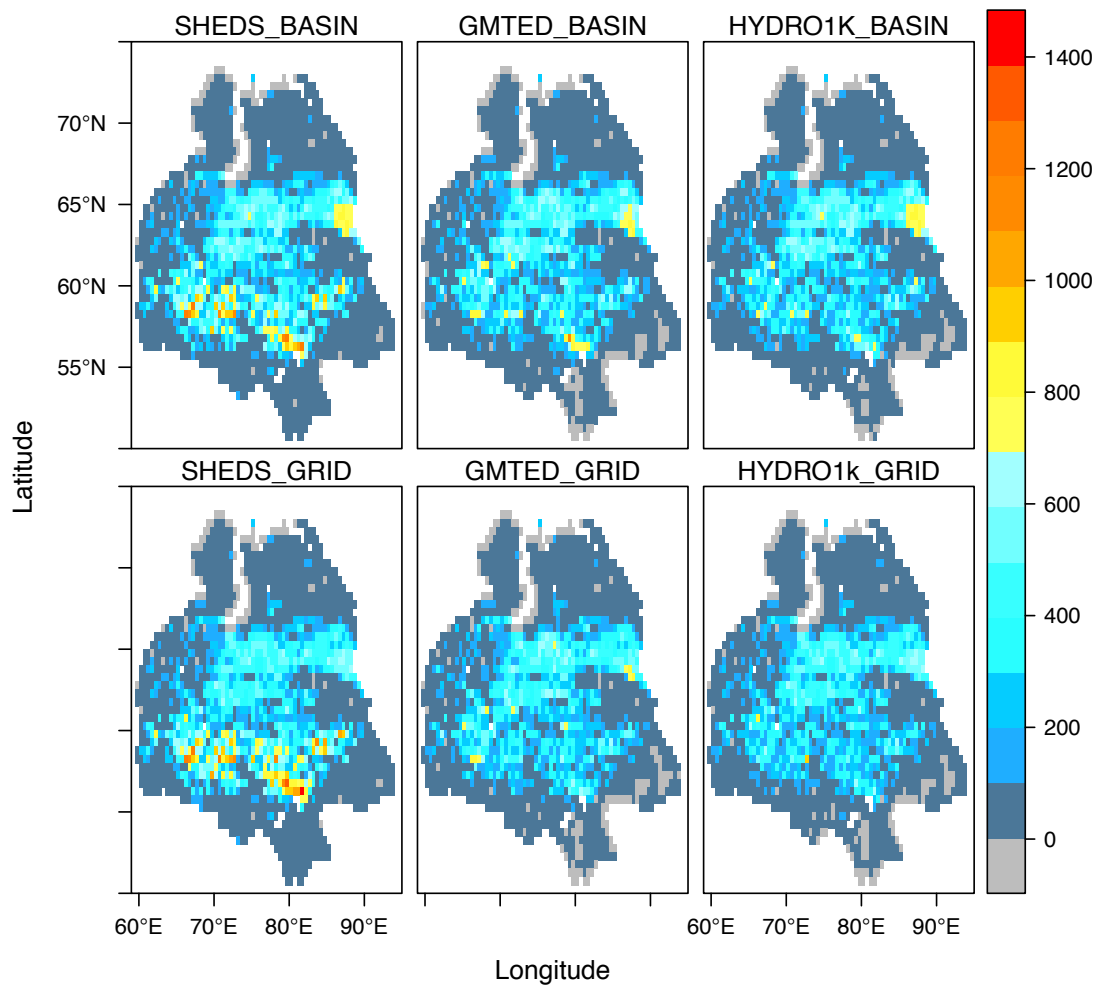
41

42



43

44 Figure 6. Observation-based estimate from Glagolev et al., 2011 and two LPJ-wsl  
 45 estimates using Hydro-SHEDS (calibrated  $F_{\max}$  and non-calibrated  $F_{\max}$ ) for  
 46 annual  $\text{CH}_4$  emission ( $\text{g CH}_4 \text{ m}^{-2} \text{ yr}^{-1}$  of grid cell area). Averages from LPJ-wsl are  
 47 over the time period 2007-2010.  
 48



49

50 Figure 7. Spatial distributions of average June-July-August (JJA) wetland area  
 51 (km<sup>2</sup>) over the West Siberian Lowland (WSL) area from model experiments (see  
 52 Table 2).

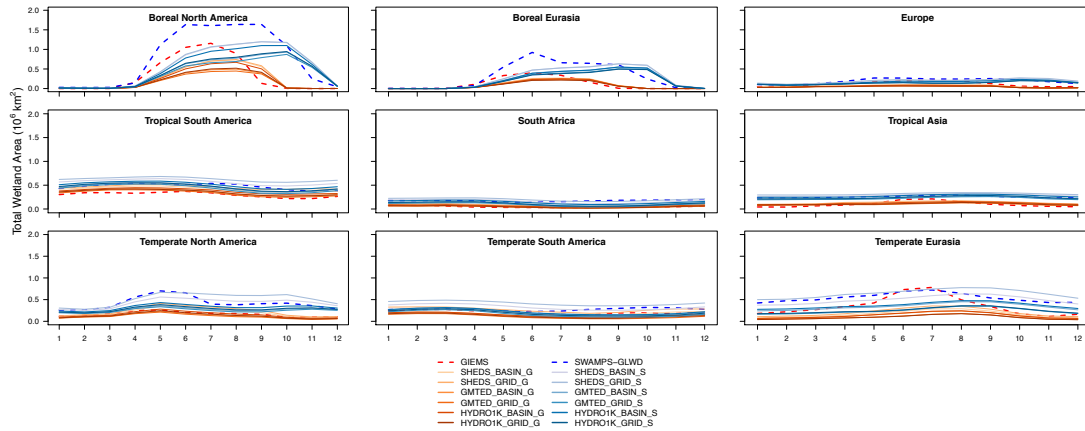


Figure 8. Average seasonal variability of observed and simulated monthly total wetland area for Transcom regions (see Fig. 2). For consistent comparison, two sets of simulated results were generated by masking out pixels for which GIEMS (red, dashed) or SWAMPS-GLWD (blue, dashed) don't have observations (denoted as 'G' and 'S', respectively).

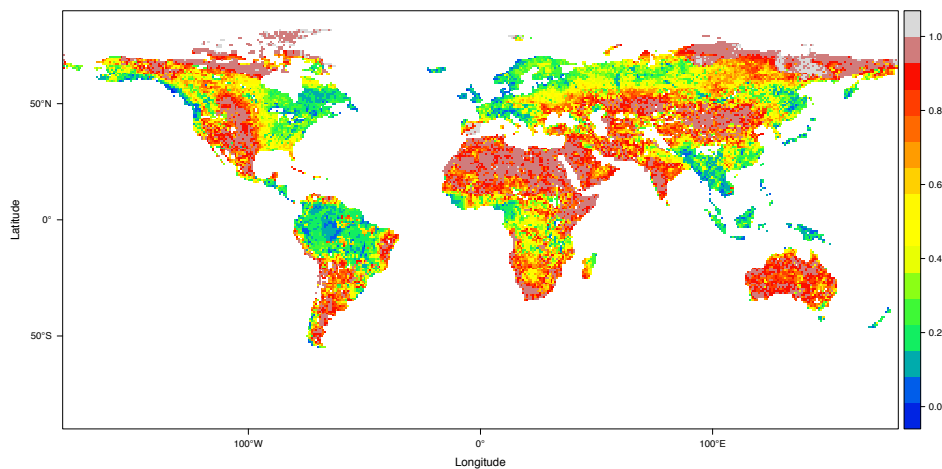
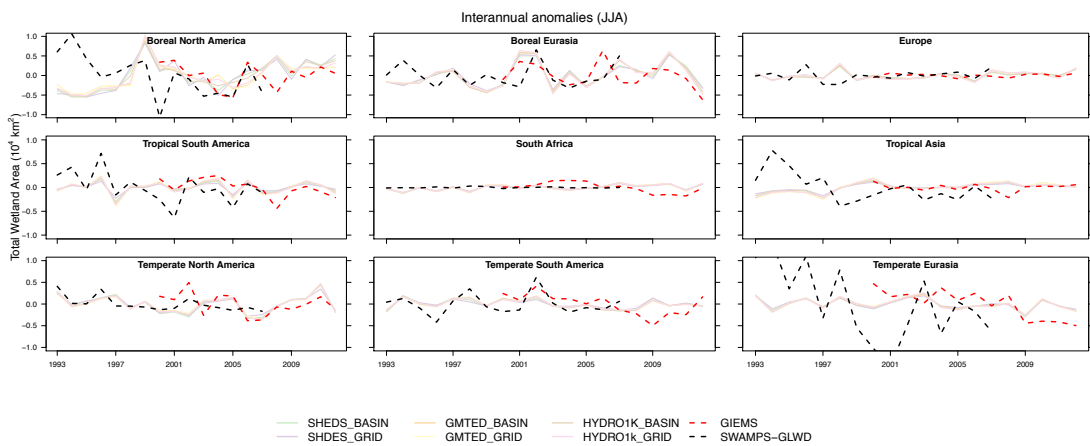
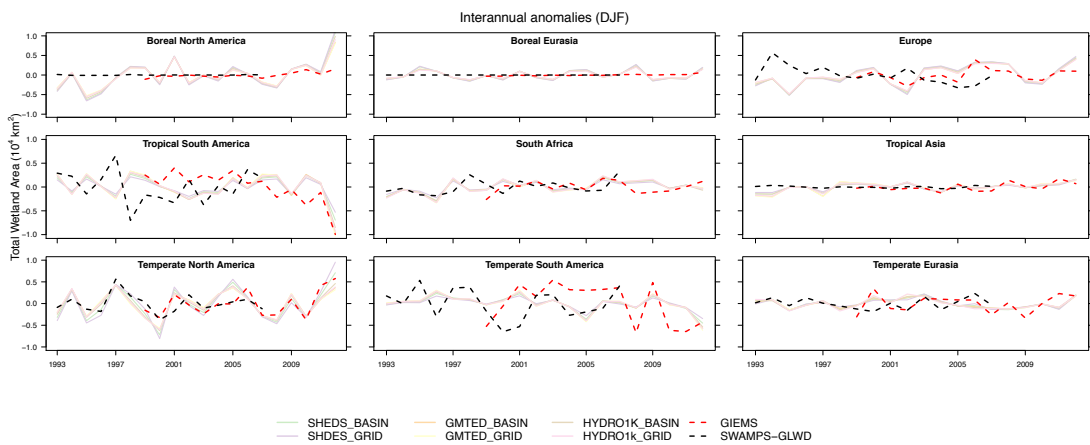
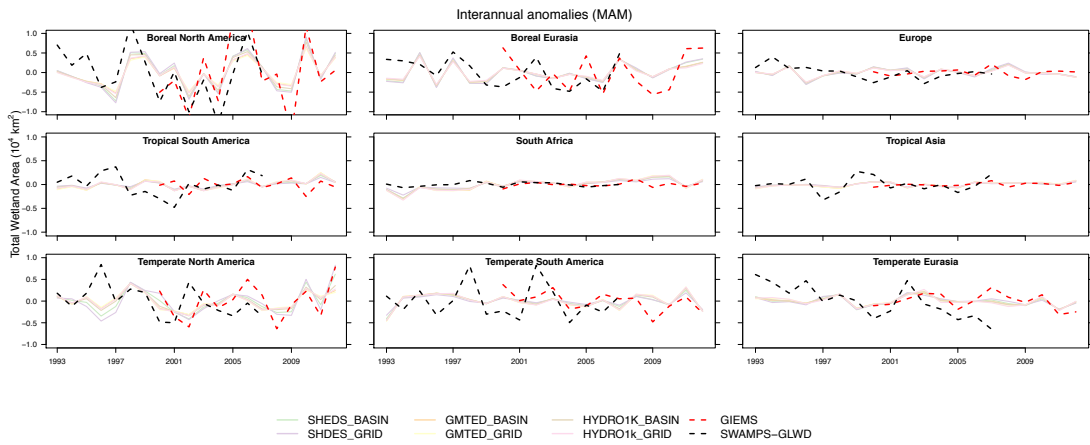


Figure 9. Global wetland potential map, which is calculated by the ratio of the mean annual maximum wetland extent averaged for the time period 1980-2010 and the long-term potential maximum wetland area ( $F_{\max}^{\text{wet}}$ ). Higher value represents higher availability for sub-grids to be inundated.

# Appendix A



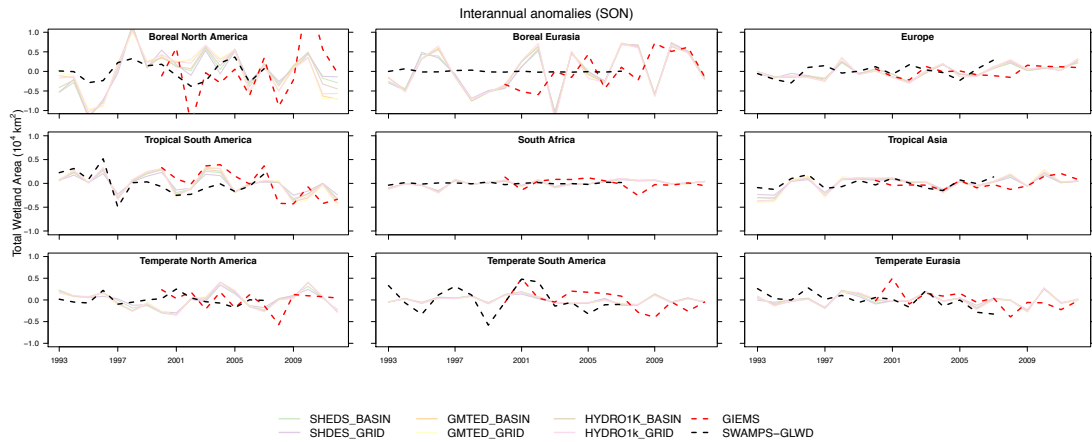


Figure A1. Interannual variations of seasonal wetland area anomalies from LPJ-wsl and satellite-derived observations for the period 1993-2012.

Table A1. Reclassification table for aggregating JERS-1 lowland Amazon basin to 0.5° cell. Code NA, 0, 1, and 2 represent Not-Available, Not Wetlands, wetland only exist in low-water season and wetland exist in high-water season.

DN	Cover at low-water stage	Cover at higher-water stage	Flag for minimum/maximum wetlands
0	Land outside Amazon Basin	Land outside Amazon Basin	NA
1	Non-wetland within Amazon Basin	Non-wetland within Amazon Basin	0
11	Open water	Open water	0
13	Open water	Aquatic macrophyte	0
21	Bare soil or herbaceous, non-flooded	Open water	2
23	Bare soil or herbaceous, non-flooded	Aquatic macrophyte	2
33	Aquatic macrophyte	Aquatic macrophyte	1
41	Shrub, non-flooded	Open water	2
44	Shrub, non-flooded	Shrub, non-flooded	0
45	Shrub, non-flooded	Shrub, flooded	2
51	Shrub, flooded	Open water	1
55	Shrub, flooded	Shrub, flooded	1
66	Woodland, non-flooded	Woodland, non-flooded	0
67	Woodland, non-flooded	Woodland, flooded	2

77	Woodland, flooded	Woodland, flooded	1
88	Forest, non-flooded	Forest, non-flooded	0
89	Forest, non-flooded	Forest, flooded	2
99	Forest, flooded	Forest, flooded	1
200	Elevation >= 500m, in Basin	Elevation >= 500, in Basin	NA
255	Ocean	Ocean	NA